



# 1 The impact of lateral boundary forcing in the CORDEX-Africa 2 ensemble over southern Africa

3

4 Maria Chara Karypidou<sup>1</sup>, Stefan Pieter Sobolowski<sup>2</sup>, Eleni Katragkou<sup>1</sup>, Lorenzo Sangelantoni<sup>3,4</sup>, Grigory Nikulin<sup>5</sup>

5 <sup>1</sup>Department of Meteorology and Climatology, School of Geology, Faculty of Sciences, Aristotle University of  
6 Thessaloniki, Thessaloniki, Greece

7 <sup>2</sup>NORCE Norwegian Research Centre, Bjerknes Centre for Climate Research, Bergen, Norway

8 <sup>3</sup>CETEMPS—Department of Physical and Chemical Sciences, University of L'Aquila, L'Aquila, Italy

9 <sup>4</sup>Department of Physical and Chemical Sciences, University of L'Aquila, L'Aquila, Italy

10 <sup>5</sup>Rosby Centre, Swedish Meteorological and Hydrological Institute, Norrköping, Sweden

11 Corresponding author: Maria Chara Karypidou, [karypidou@geo.auth.gr](mailto:karypidou@geo.auth.gr)

12

## 13 Abstract

14

15 The region of southern Africa (SAF) is among the most exposed climate change hotspots and is projected to experience  
16 severe impacts on multiple economical and societal sectors. For this reason, producing reliable projections of the  
17 expected impacts of climate change is key for local communities. In this work we use a set of 19 regional climate  
18 models (RCMs) performed in the context of the Coordinated Regional Climate Downscaling Experiment (CORDEX)  
19 – Africa and a set of 10 global climate models (GCMs) participating in the Coupled Model Intercomparison Project  
20 Phase 5 (CMIP5), that were used as the driving GCMs in the RCM simulations. We are concerned about the degree  
21 to which RCM simulations are influenced by their driving GCMs, with regards to monthly precipitation climatologies,  
22 precipitation biases and precipitation change signal, according to the Representative Concentration Pathway (RCP)  
23 8.5 for the end of the 21st century. We investigate the degree to which RCMs and GCMs are able to reproduce specific  
24 climatic features over SAF and over three sub-regions, namely the greater Angola region, the greater Mozambique  
25 region and the greater South Africa region. We identify that during the beginning of the rainy season, when regional  
26 processes are largely dependent on the coupling between the surface and the atmosphere, the impact of the driving  
27 GCMs on the RCMs is smaller, compared to the core of the rainy season, when precipitation is mainly controlled by  
28 the large-scale circulation. In addition, we show that RCMs are able to counteract the bias received by their driving  
29 GCMs, hence, we claim that the cascade of uncertainty over SAF is not additive, but indeed the RCMs do provide  
30 improved precipitation climatologies. The fact that certain bias patterns over the historical period (1985-2005)  
31 identified in GCMs are resolved in RCMs, provides evidence that RCMs are reliable tools for climate change impact  
32 studies over SAF.

33

34

35

36



## 37 **1 Introduction**

38

39 The region of southern Africa (SAF) is among the most exposed climate change hotspots (Diffenbaugh and Giorgi,  
40 2012), and is projected to experience severe impacts on multiple economical and societal sectors (Conway et al., 2015;  
41 Masipa, 2017; Shew et al., 2020). Poverty, food insecurity and high levels of malnutrition (Misselhorn and Hendriks,  
42 2017) render SAF a region particularly vulnerable to the impacts of climate change (Casale et al., 2010; Luan et al.,  
43 2013; Wolski et al., 2020). In addition, the population's reliance on rain-fed agriculture makes strategic planning  
44 necessary as it aims to mitigate the impact of climate change on local communities.

45 Global climate models (GCM) participating in the Coupled Model Intercomparison Project Phase 5 (CMIP5) (Taylor  
46 et al., 2012) project a significant decline in annual precipitation over SAF (IPCC and Stocker, 2013), with the most  
47 pronounced changes projected under representative concentration pathway 8.5 (RCP8.5) (Sillmann et al., 2013). This  
48 reduction is also identified in the regional climate model (RCM) simulations performed in the context of the  
49 Coordinated Regional Climate Downscaling Experiment (CORDEX) – Africa domain (Nikulin et al., 2012; Giorgi  
50 and Gutowski, 2015). More specifically according to CORDEX-Africa simulations, annual precipitation is expected  
51 to decline by up to 50% by the end of the 21<sup>st</sup> century (Pinto et al., 2018), while duration of dry spells is projected to  
52 increase (Dosio et al., 2019). Despite this, extreme rain events are expected to increase in frequency and intensity  
53 (Pinto et al., 2016; Abiodun et al., 2019). Nevertheless, for a global warming level of 2 °C, certain parts of SAF  
54 (northern Angola, Zambia, northern Mozambique and eastern South Africa) are projected to experience precipitation  
55 increase during specific times of the year (Maúre et al., 2018).

56 The question of whether or not RCMs produce demonstrable added value relative to their driving GCMs, has often  
57 fueled debate between the RCM and GCM modelling communities (Lloyd et al., 2020). The outcome of the debate is  
58 not binary. The literature provides ample evidence that there is indeed evidence of added value in RCMs, but it is  
59 dependent on the region examined, on the season and the climate mechanisms that are at play (Luca et al., 2016, Feser  
60 et al., 2011). RCM ensembles such as those in CORDEX-Africa endeavor to provide added value, by dynamically  
61 downscaling historical and scenario simulations originating from coarse resolution GCMs (Dosio et al., 2019). The  
62 added value in RCM simulations arises as a result of their higher horizontal resolution (<50 km), which makes it  
63 possible for atmospheric waves and synoptic scale disturbances to be represented in a more realistic manner. An  
64 additional aspect that further contributes towards this end, is the more accurate representation of land surface  
65 characteristics (topography, land use etc.) in RCMs (Di Luca et al., 2013). Moreover, the physics of a RCM can be  
66 targeted for processes specific to the region it is being run for, giving it a local advantage over GCMs that may have  
67 had their physics developed for global applications. Nevertheless, RCMs also are accompanied by a set of model  
68 deficiencies of their own that affect the final output of the downscaled data (Boberg and Christensen, 2012). In Sørland  
69 et al. (2018) it is reported that although RCM biases are affected by the driving GCMs, they are nonetheless not  
70 additive, a result that counters the common “cascade of uncertainty” criticism. Still, uncertainty arising from both the  
71 driving GCM and the downscaling RCM affect the final product, and it is important to diagnose the sources and causes  
72 of these errors (Déqué et al., 2012).



73 Attributing this uncertainty into its respective components is key for a better assessment of the reliability of RCM  
74 simulations (Christensen and Kjellström, 2020). GCMs provide the lateral boundary conditions to the RCMs and each  
75 RCM receives, absorbs, and modulates the received atmospheric forcing in different ways, depending on the numerical  
76 formulations and parameterization schemes employed. Discerning between the signal received by the GCM and the  
77 signal produced by the RCM is critical for assessing the robustness with which different modelling systems are able  
78 to accurately reproduce observed climatologies and generate reliable estimates of the expected climate change. In  
79 addition, the manner in which an RCM responds to the atmospheric forcing provided by a GCM can be region specific  
80 (Rana et al., 2020; Wu and Gao, 2020) (e.g., regions located in close proximity to the boundaries of the RCM domain  
81 can be more severely affected by the driving GCMs, than regions at the center of the RCM domain or there can be  
82 region specific response around complex topography versus lowlands). Also, the degree to which an RCM is  
83 influenced by the driving GCM can be process specific. For instance, when there is a strong large-scale circulation  
84 signal that is introduced to an RCM domain (e.g. advective mid-latitude storms), it is quite likely that the RCM will  
85 be able to reproduce the information that is received at its lateral boundaries. If, however, the large-scale forcing is  
86 weak, then the atmospheric conditions simulated within the RCM domain are more dependent on the dynamic and  
87 thermodynamic processes employed by the RCM (e.g. convective thunderstorms).

88 In this work we aim to assess whether it is the RCMs or their driving GCMs that dominate monthly precipitation  
89 climatology, monthly precipitation bias and climate change signal over SAF. We take into account the region-specific  
90 characteristics of this question by analyzing SAF and three subregions, namely southeastern Angola, Mozambique  
91 and South Africa. We also consider the different atmospheric processes that are in play over each region by analyzing  
92 monthly climatologies. Precipitation over SAF results from various atmospheric processes that are highly variable  
93 during the rainy season (Oct-Mar), so by performing the analysis on a monthly basis, we are able to indirectly study  
94 how certain processes are reproduced by GCM and RCM simulations. In order to differentiate between the signal  
95 emanating from the RCMs and their driving GCMs, we use the analysis of variance (ANOVA) in both the GCM and  
96 the RCM ensembles (Déqué et al., 2007, 2012). Since the information provided by RCMs will eventually be used by  
97 both climate and non-climate scientists, especially in light of climate change impact studies, we aim to provide some  
98 information with regards to how much each RCM output is affected by its driving GCM and what climate change  
99 signals are identified consistently in both RCMs and GCMs.

100

## 101 **2 Material and methods**

### 102 **2.1 Data**

103 The data analyzed in the current work are displayed in **Table 1** and consist of RCM simulations performed in the  
104 context of CORDEX-Africa, a set of simulations performed in the context of CMIP5, and the CHIRPS satellite rainfall  
105 product (Funk et al., 2015). More specifically, the CORDEX-Africa simulations selected are those that were driven  
106 by more than two GCMs and for which there are runs for both the historical and the future period under RCP8.5. The  
107 CMIP5 GCMs selected are the ones that were used to drive the CORDEX-Africa simulations. All RCM and GCM  
108 simulations were retrieved from the Earth System Grid Federation (<https://esgf-data.dkrz.de/projects/esgf-dkrz/>). The



109 CHIRPS rainfall product is used for calculating precipitation biases in both the CORDEX-Africa and CMIP5  
 110 ensembles and was retrieved from: <https://www.chc.ucsb.edu/data/chirps>. CHIRPS is available at 5 km spatial  
 111 resolution and for the calculation of biases it was remapped to the coarser resolution grid using conservative  
 112 remapping.

113 Our analysis is split into two sections: the qualitative and the quantitative part. In the qualitative part, we aim to  
 114 identify if RCMs exhibit systematic behavior relative to their driving GCMs. For the quantitative part, we aim to  
 115 quantify the degree to which monthly precipitation climatologies, biases and climate change signals are affected by  
 116 the downscaled RCMs or by the GCMs driving the RCM simulations. For this purpose, we employ an ensemble of 19  
 117 RCM simulations driven by 10 GCMs and the driving GCMs that were used to provide the lateral boundary conditions  
 118 to the RCMs. From the historical simulations we use the period 1985-2005 and from the projection simulations we  
 119 use the period 2065-2095 under RCP8.5. All CORDEX-Africa simulations are available at ~50 km horizontal  
 120 resolution, while the horizontal resolution for the driving GCMs is provided in **Table 2**.

121

122 **Table 1** Input RCM and GCM simulations used. The CORDEX-Africa simulations are given in the columns. The  
 123 CMIP5 GCMs used as driving fields are given in the rows.

	<b>CCLM4-8-17.v1</b>	<b>RCA4.v1</b>	<b>REMO2009.v1</b>
<b>CanESM2</b>		√	
<b>CNRM-CM5</b>	√	√	
<b>EC-EARTH</b>	√	√	√
<b>HadGEM2-ES</b>	√	√	√
<b>MIROC5</b>		√	√
<b>MPI-ESM-LR</b>	√	√	√
<b>IPSL-CM5A-LR</b>			√
<b>IPSL-CM5A-MR</b>		√	
<b>CSIRO-Mk3-6-0</b>		√	
<b>GFDL-ESM2M</b>		√	
<b>NorESM1-M</b>		√	

124

125 **Table 2** Horizontal resolution of the CMIP5 GCMs used as driving fields in the CORDEX-Africa simulations.

<b>GCMs</b>	<b>Latitude Res.</b>	<b>Longitude Res.</b>	<b>References</b>
<b>CanESM2</b>	2.7906°	2.8125°	(CCCma, 2017)
<b>CNRM-CM5</b>	1.40008°	1.40625°	(Voldoire et al., 2013)
<b>CSIRO-Mk3-6-0</b>	1.8653°	1.875°	(Jeffrey et al., 2013)
<b>EC-EARTH</b>	1.1215°	1.125°	(Hazeleger et al., 2010)
<b>GFDL-ESM-2M</b>	2.0225°	2.5°	(Dunne et al., 2012)
<b>HadGEM2-ES</b>	1.25°	1.875°	(Collins et al., 2011)
<b>IPSL-CM5A-MR</b>	1.2676°	2.5°	(Dufresne et al., 2013)
	1.894737°	3.75°	
<b>IPSL-CM5A-LR</b>			
<b>MIROC5</b>	1.4008°	1.40625°	(Watanabe et al., 2010)
<b>MPI-ESM-LR</b>	1.8653°	1.875°	(Giorgetta et al., 2013)
<b>NorESM1-M</b>	1.894737°	2.5°	(Bentsen et al., 2013)



## 126 2.2 Methods

127 The study region and subregions considered are depicted in **Fig. 1**. The subregions are selected based on particular  
128 phenomena and processes that are of importance for the seasonal cycle of precipitation. More specifically, Region A  
129 encompasses the entire SAF region and is defined as the area extending from 10 °E to 42 °E and from 10 °S to 35 °S.  
130 Region B was selected to capture the main region of interest with regards to the Angola Low (AL) pressure system  
131 (Howard and Washington, 2018) and covers the area extending from 14 °E to 25 °E and from 11 °S to 19 °S. Region  
132 C covers the eastern coastline, Mozambique and surrounding countries and extends from 31 °E to 41 °E and from 10  
133 °S to 28 °S. Lastly, we define Region D, which covers much of South Africa and extends from 15 °E to 33 °E and  
134 from 26 °S to 35 °S.

135 One of the primary synoptic scale features controlling precipitation over SAF is the Angola Low (AL) pressure system  
136 (Reason and Jagadheesha, 2005; Lyon and Mason, 2007; Crétat et al., 2019; Munday and Washington, 2017; Howard  
137 and Washington, 2018), which has a distinct seasonal cycle throughout the rainy season (Oct-Mar). This motivates its  
138 selection as a subregion for our study. The AL exhibits heat low characteristics during Oct-Nov and tropical low  
139 characteristics during Dec-Feb (Howard and Washington, 2018). This suggests that during Oct-Nov, since  
140 precipitation is thermally induced and thus tightly dependent on land-atmosphere interactions, it will be the RCMs  
141 that are dominant in controlling precipitation processes. As the rainy season progresses, the AL changes to a tropical  
142 low pressure system and its formation is controlled by the large-scale circulation that is characterized by easterly  
143 winds from the Indian Ocean that enter SAF via the Mozambique channel. Since precipitation during Dec-Feb is  
144 caused by transient low-pressure systems, we hypothesize that the impact of the driving GCM fields during Dec-Feb  
145 is enhanced.

146 In addition, the wider area of Mozambique is a region where the majority of tropical cyclones/depressions make  
147 landfall over continental SAF. The occurrence of transient low-pressure systems is enhanced during the core of the  
148 rainy season (Dec-Feb) and thus we are interested in identifying whether the impact of the driving GCMs is dominant  
149 during Dec-Feb. Also, since according to (Muthige et al., 2018), the number of landfalling tropical cyclones under  
150 RCP8.5 is expected to decline in the future, we are interested in examining whether the impact of the driving GCMs  
151 to the RCM simulations will be altered under future conditions. Hence, Region C is used as a region indicative of the  
152 landfalling tropical cyclones/depressions. Lastly, we examine the area encompassing South Africa (Region D) due to  
153 its strong land-ocean gradients, complex topography and strong seasonal variations in rainfall zones.

154

### 155 2.2.1 Monthly precipitation climatology and bias

156 In order to assess whether or not the RCMs improve the monthly precipitation climatologies relative to their driving  
157 GCMs, we employ a method initially described in Kerkhoff et al. (2015) and later employed by Sørland et al. (2018),  
158 which displays in a scatterplot form the RCM increment as a function of the GCM bias. More specifically, the RCM  
159 increment is described as the difference of each RCM simulation from its driving GCM (RCM-GCM). The RCM  
160 increment is plotted against the GCM bias (GCM-OBS). This plot displays whether or not the RCM increment  
161 counteracts the GCM bias. If the RCM increment reduces the GCM bias, then points are expected to lie along the  $y=-x$   
162 line (negative correlation). On the contrary, if the RCM increment increases the GCM bias, then points are expected



163 to lie along the  $y=x$  line (positive correlation). If the RCM increment and the GCM bias are independent, then points  
164 are expected to be scattered randomly.

165

### 166 2.2.2 Climate change signal

167 The climate change signal (CCS) is identified as the monthly mean difference between the future period (2065-2095)  
168 minus the historical period (1985-2005). As an exploratory method of inspecting the differences between each RCM  
169 simulation from its respective driving (GCM) for monthly precipitation during both the historical and the future period,  
170 we subtract the downscaled precipitation field ( $RCM_{DRI}$ ) from its driving ( $DRI$ ), as in **Eq. 1**:

$$DIFF = RCM_{DRI} - DRI \quad \text{Eq. 1}$$

171 If  $DIFF > 0$ , then we assume that the RCM enhances precipitation, relative to its driving GCM, while if  $DIFF < 0$  then  
172 we assume that the RCM reduces precipitation, relative to its driving GCM. This method is employed in the qualitative  
173 part of the analysis.

174

### 175 2.2.3 Analysis of variance

176 Additionally, we employ an ANOVA decomposition (Déqué et al., 2007, 2012), in order to understand whether it is  
177 the RCMs or their respective driving GCMs that are responsible for controlling precipitation over the historical (1985-  
178 2005) period and the future period (2065-2095). For this purpose, we use two quantities, namely the “inter-RCM”  
179 variance and the “inter-GCM” variance, as in (Déqué et al., 2012). More specifically, the “inter-RCM variance” is the  
180 variance between all the RCM simulations that are driven by the same GCM. Subsequently, all variances obtained for  
181 all driving GCMs are averaged.

$$RCM_{var} = \frac{1}{N_{RCM}} \sum_{RCM_j} (P_{ij} - \underline{P}_j)^2 \quad \text{Eq. 2}$$

182 The quantity  $P_{ij}$  is the monthly precipitation obtained from all RCMs ( $j$ ) that were driven by the same GCM ( $i$ ). The  
183 quantity  $\underline{P}_j$  is the mean monthly precipitation obtained by all RCMs ( $j$ ) that share a common driving GCM ( $i$ ). As a  
184 final step, the average of all variances is calculated.

$$Inter\_RCMvar = \frac{\sum GCM_i}{N} \quad \text{Eq. 3}$$

185 Similarly, the “inter-GCM” variance describes the variance between all the GCMs that were used to drive a single  
186 RCM and then averaged over all the variances obtained for all driven RCMs.

$$GCM_{var} = \frac{1}{N_{GCM}} \sum_{GCM_i} (P_{ij} - \underline{P}_i)^2 \quad \text{Eq. 4}$$

187 Likewise, the average of all variances is calculated.

$$Inter\_GCMvar = \frac{\sum RCM_i}{N} \quad \text{Eq. 5}$$

188 Both “inter-RCM” and “inter-GCM” variances are normalized by the total variance obtained for all months, as in  
189 (Vautard et al., 2020), so that all values, both for historical and projection runs and RCM and GCM simulations are  
190 comparable. A schematic of the process described above is provided in **Fig. S1**.



### 191 3 Results

192 The October and January precipitation climatologies for the period 1985-2005 are displayed in **Fig. 2** and **Fig. 3**,  
193 respectively. We use October and January climatologies, because these 2 months may be considered representative  
194 of the distinctive processes controlling precipitation over SAF (see section 2.2). We avoid using seasonal means, since  
195 the temporal averaging of precipitation often obscures attributes that are better identified on a monthly level. The  
196 remaining months of the rainy season are shown in the supplementary material. More specifically, we use October as  
197 it is the month that heralds the onset of the rainy season and is often associated with weak precipitation and convective  
198 processes that are mainly due to excess surface heating. Also, it is during October that the most intense formations of  
199 the heat low expression of the AL are observed. Likewise, we use January as it represents the core of the rainy season,  
200 with very strong large-scale precipitation, mainly from the southeastern (SE) part of SAF, through transient synoptic  
201 scale low pressure systems.

202 As it is displayed in **Fig. 2**, precipitation during October occurs in the northwestern (NW) part and the SE part of SAF.  
203 Precipitation in the NW part is associated with the southward migration of the rainband (Nicholson, 2018), while  
204 precipitation over the SE part is associated with an early formation of the tropical temperate troughs (TTTs). As it is  
205 evident from **Fig. 2**, CCLM4-8-17.v1 reduces precipitation amounts (approximately 4-5 mm/d) in both the NW and  
206 SE parts of SAF, relative to the lateral boundary forcing it receives. On the contrary, RCA4.v1 systematically enhances  
207 precipitation amounts, regardless of the driving GCM. Also, precipitation according to RCA4.v1 displays a very  
208 localized spatial pattern with very strong spatial heterogeneity. This may be attributed to the fact that the topography  
209 is not smoothed enough and leads to high precipitation values over grid boxes with high elevation (Van Vooren et al.,  
210 2019). This is particularly evident in the mountainous region over coastal Angola. REMO2009.v1 also enhances  
211 precipitation amounts regardless of the driving GCM, however in a much more spatially homogeneous way than  
212 RCA4.v1.

213  
214 As it is shown in **Fig. 3**, high precipitation amounts during January are observed over the northern and eastern regions  
215 of SAF. During January, differences among the driving GCMs become more pronounced, however, all models agree  
216 on the dry conditions observed over the southwestern (SW) part of SAF. With regards to the downscaled products,  
217 CCLM4-8-17.v1 produces high precipitation amounts over the central part of northern SAF but displays varying  
218 amounts of precipitation over the coastal parts, depending on the driving GCM. RCA4.v1 downscales precipitation in  
219 a very localized pattern and enhances precipitation over areas with steep terrain. Also, precipitation over the lake  
220 Malawi region is particularly enhanced, regardless of the driving GCM. REMO2009.v1 displays similar precipitation  
221 amounts to its driving GCMs, however it enhances precipitation over the coastal part of Angola and Mozambique and  
222 yields excess precipitation over lake Malawi, when it is driven by HadGEM2-ES and IPSL. The monthly climatologies  
223 for the rest of the rainy season months are shown in the supplementary material (**Fig. S2 – S5**).

224  
225  
226



227 In **Fig. 4** the monthly precipitation bias for October over SAF is shown. Biases are calculated using the CHIRPS  
228 satellite rainfall product as a reference. With the exception of IPSL-CM5A (LR/MR) and CanESM2, all other GCMs  
229 display a consistent wet bias that ranges from 0.1 – 30 mm/d (in isolated areas), with most values over SAF falling  
230 0.1-3 mm/d. Overall, the same pattern generally holds for RCA4.v1 and REMO2009.v1, while CCLM4-7-18.v1  
231 displays a systematic dry bias that reaches 2 mm/d, when forced with EC-EARTH, MPI-ESM-LR and HadGEM2-ES.  
232 More specifically, concerning RCA4.v1, the region where the highest wet bias is observed is over Region B (the  
233 Angola Low region) and over the NW parts of coastal Angola. The dry bias regions in RCA4.v1 are identified over  
234 the northeastern (NE) and southern parts of SAF and they rarely exceed -1.5 mm/d.

235 The monthly precipitation biases for January over SAF are shown in **Fig. 5**. There is a prevailing wet bias identified  
236 in almost all GCMs that typically reaches 3 - 3.5 mm/d, however, in MIROC5, NorESM and GFDL-ESM2M the  
237 biases exceed 5 mm/d over a major part of SAF. Another feature that systematically appears in GCMs is a dry bias  
238 over the NE part of SAF. This bias pattern is also identified in almost all RCMs with a systematic wet bias over central  
239 and western SAF and a region of dry bias in the NE part. More specifically, in RCA4.v1 and REMO2009.v1, there is  
240 a dry bias over the NE and the southern coast of SAF, while in CCLM4-7-18.v1 the dry bias over the eastern region  
241 extends inland to cover almost the whole of Mozambique. Another interesting feature is identified around the Angolan  
242 coast, where wet biases exceed 5 mm/d, while over an adjacent region there is a strip of dry biases that reaches 2  
243 mm/d. Considering the abrupt increase in elevation and the steep escarpment over the coastal Angola-Namibia region,  
244 this is possibly caused by local circulation driving excess moisture transport from the Atlantic Ocean and overly  
245 aggressive orographically triggered precipitation on the windward side of the topography (wet bias strip), that leads  
246 to dry conditions in the lee side (dry bias strip) (Howard and Washington, 2018). It is noted that the wet bias over the  
247 coastal region is identified in most of the RCA4.v1 simulations and in all REMO2009.v1 simulations, however, the  
248 dry bias in the lee side is seen in CCLM4-7.18.v1 only. The monthly precipitation biases for the rest of the rainy  
249 season months is shown in the supplementary material (**Fig. S6 – S9**).

250

251 A more detailed look into specific subregions over SAF where certain climatological features and processes are at  
252 play, can help gain a more in-depth insight of how the precipitation biases are distributed during each month of the  
253 rainy season and whether or not the RCMs display any improvement relative to their driving GCMs. For this reason,  
254 we plot the RCM increments (RCM-GCM) as a function of the GCM biases (GCM-OBS). The results for October  
255 over SAF and the 3 subregions are displayed in **Fig. 6**. In general, all points are identified close to the  $y=-x$  line, hence  
256 there is a tendency that RCMs systematically counteract GCM biases. There are nonetheless substantial differences  
257 between the four regions. For instance, over Region A (SAF region) the IPSL-MR GCM has a wet bias equal to almost  
258 1 mm/day, which is counteracted by RCA by an increment of -0.4 mm/month. Other RCA simulations when driven  
259 by HadGEM2-ES, CNRM-CM5 or EC-EARTH, display an RCM increment similar to that of the GCM bias, hence  
260 RCMs mitigate the GCM bias. Over Region B (Angola Low region) most of the RCMs display an RCM increment  
261 that is nearly equal to the GCM bias. Similar conclusions are drawn for Regions C and D also. The RCM increments  
262 as a function of the GCM biases for January are shown in **Fig. 7**. For all regions except Region D (South Africa) points



263 are lying closely to the  $y=-x$  line, hence overall, RCM increments counteract the GCM biases. The scatterplots for the  
264 rest of the months of the rainy season are shown in the supplementary material (**Fig. S10 – S13**). In general, although  
265 precipitation in RCMs is strongly dependent on the driving GCMs, the RCM increments are anticorrelated to the GCM  
266 biases. The anticorrelations are particularly strong for the Dec-Mar period of the rainy season over Region A, B and  
267 C, but not over D (**Fig. S14**).

268 In **Fig. 8** the mean analysis of variance of all RCMs driven by the same GCM and of all GCMs driving the same RCM  
269 is shown. Values are spatially averaged for southern Africa and the 3 subregions examined (land pixels only) and refer  
270 to the period 1985-2005. In Region A, monthly precipitation during October and November is dominated by the  
271 RCMs, while during Jan-Mar, it is the GCMs that play a dominant role in formulating precipitation over SAF. This is  
272 indicative of the impact that RCMs exert on the formulation of precipitation during Oct-Nov-Dec and the fact that the  
273 contribution from the GCMs becomes dominant during Jan-Feb-Mar. The fact that the contribution of RCMs during  
274 Oct-Nov-Dec dominates can be attributed to the fact that precipitation during these months is the result of regional  
275 processes that are largely dependent on the coupling between the surface and the atmosphere. The land-atmosphere  
276 coupling is a characteristic resolved by the RCMs, through mechanisms described in land surface models, planetary  
277 boundary layer schemes, convection schemes etc., making the contribution of the large scale drivers from the GCM  
278 less important. However, during Jan-Feb-Mar we observe that the contribution from the RCMs is reduced, and it is  
279 the GCMs that control the monthly precipitation variability. This can be attributed to the fact that during Jan-Feb-Mar  
280 it is the large-scale circulation that modulates precipitation over SAF and the GCMs control the transient synoptic  
281 scale systems that enter SAF. In Region B, the pattern is similar, however, October and November precipitation are  
282 closer to the diagonal, indicating an almost equal contribution by both RCMs and GCMs. Also, Dec-Feb move closer  
283 to the diagonal, nevertheless, precipitation during March is mainly formulated by GCMs. In Region C, October  
284 remains equally influenced by both RCMs and GCMs, however November and December are dominated by the  
285 influence of the RCMs. In Region D, precipitation for all months except October is influenced by GCMs.

286 In **Fig. 9** the climate change signal for October precipitation over SAF is depicted. All GCMs agree that October  
287 precipitation will decline by approximately 2 mm/d over the regions that experience precipitation during this period,  
288 namely the NW and SE parts of SAF. In addition, some GCMs display a minor precipitation increase (0 - 0.5 mm/d)  
289 in the SW part of SAF, while some others display a slightly larger (1.5 mm/d) precipitation increase over the eastern  
290 parts of South Africa. Moreover, it is seen that the precipitation change signal is replicated by almost all the  
291 downscaling RCMs, nevertheless, there are some considerable differences between the RCMs and their driving GCM.  
292 More specifically, RCA4.v1 in almost all simulations, displays a larger reduction of the precipitation change signal  
293 relative to its driving GCM, both in magnitude and in spatial extent. Precipitation changes in CCLM4-8-17.v1 seem  
294 to follow closely the driving GCMs, with a severe exception when CNRM-CM5 is used (the NW part of SAF  
295 experiences precipitation decline almost 4 mm/d larger than in the driving GCM). The case for when CCLM4-8-17.v1  
296 is driven by CNRM-CM5 may be partly caused by the fact that the historical simulation had erroneously used lateral  
297 boundary conditions from a different simulation member of CNRM-CM5 (Vautard et al., 2020). In REMO2009.v1, a  
298 precipitation decline region is identified in the NW part of SAF and a minor precipitation increase over eastern South



299 Africa is identified. This pattern for REMO2009.v1 appears to be consistent, regardless of the driving GCM, which  
300 could be partly explained by the fact that precipitation during October is thermally driven, and thus the impact of the  
301 driving GCMs is not dominant. The precipitation increase in the SE part of SAF is seen over a localized region and  
302 could be associated with an increase in the precipitation caused by the Tropical Temperate Troughs (TTTs) (Ratna et  
303 al., 2013; Macron et al., 2014; Shongwe et al., 2015).

304 In **Fig. 10** the climate change signal for precipitation during January is displayed. The precipitation change displays a  
305 very strong regional heterogeneity. It is also observed that although there is a strong precipitation change signal in all  
306 driving GCMs, not all RCMs downscale the signal uniformly. It is also notable that, even among the GCMs, there are  
307 substantial differences in the spatial extent and sign of the change. Nevertheless, there are some features that appear  
308 in most of the simulations. For instance, almost all GCMs project drying conditions over the SW part of SAF,  
309 especially the coastal zone. The precipitation decline is equal to -1 mm/d. This could be explained by a consistent  
310 increase in frequency of the Benguela Coastal Low-Level Jet events (Lima et al., 2019; Reboita et al., 2019), causing  
311 oceanic upwelling and a subsequent reduction in precipitation. In addition, there is a subset of GCMs that identify a  
312 severe precipitation decline over the Angola region that reaches -5 mm/d. Furthermore, in many GCMs a region of  
313 precipitation increase is identified, extending from central SAF towards SE SAF. This is particularly identifiable in  
314 HadGEM2-ES, and the RCM simulations forced by it. The monthly precipitation changes for the rest of the rainy  
315 season months is shown in the supplementary material (**Fig. S15 – S18**).

316 In **Fig. 11** the spatial average of the  $RCM_{DRI} - DRI$  difference (DIFF) is shown for the whole of SAF (land pixels  
317 only). If  $DIFF > 0$ , it indicates that the RCMs enhance precipitation relative to their driving GCM, while if  $DIFF < 0$   
318 then RCMs reduce precipitation relative to their driving GCM. As it is shown, DIFF values for October are symmetric  
319 around zero and do not exceed the range  $(-1) - 1$  mm/d, either for the historical or the future period. Almost symmetric  
320 are the DIFF values for November also, however, their spread increases, reaching values that range  $(-2) - 2$  mm/d. In  
321 both months, CCLM4-7-18.v1 always reduces precipitation amounts relative to the lateral boundary forcing it  
322 receives, regardless of the driving GCM or the period examined. During December, the precipitation reduction in all  
323 RCMs becomes more pronounced and reaches values equal to -3 mm/d. In January, only 1 RCM enhances  
324 precipitation ( $\sim 0.5$  mm/d) with all the rest displaying precipitation reduction. During February and March, some  
325 positive DIFF values re-appear for some simulations. Overall, there is a strong linear relationship between DIFF in  
326 1985-2005 and 2065-2095, which further implies that if an RCM is drier than its driving GCM during the historical  
327 period, then it will retain this attribute during the future period also. Nonetheless, we highlight that RCMs preserve  
328 precipitation change signal generated by the GCMs. Considering that one primary shortcoming of the GCMs over  
329 SAF is their wet bias and that RCMs systematically reduce this bias, we gain increased confidence that RCMs can be  
330 reliably used for future projections with regards to precipitation change.

331 In **Fig. 12** the spatial average of the precipitation change signal from RCMs and their driving GCMs relative to 1985-  
332 2005 for SAF and the 3 subregions is displayed. Concerning Region A, all models during October identify a  
333 precipitation reduction at the end of the 21<sup>st</sup> century that can reach -0.9 mm/d. The precipitation decline signal is also  
334 identified during November, indicating a later onset of the rainy season over SAF, as it has already been shown for



335 CMIP5 (Dunning et al., 2018). During December and January there is a variability in the spatial averages of the change  
336 signal that ranges from -0.8 to 0.8 mm/d. A similar pattern is also seen for February and March. The distribution of  
337 the ensemble members for both RCMs and GCMs in Regions B and C is similar to that of Region A, however in  
338 Regions B and C precipitation change values display a considerably larger spread. In Region D the climate change  
339 signal is symmetric around 0 for all months, except March.

340 The impact the RCMs and GCMs on monthly precipitation for the period 2065-2095 under RCP8.5 is shown in **Fig.**  
341 **13**. Regions A and B show a similar behavior as in the historical period (**Fig. 8**), however, in Region C, precipitation  
342 during March is more strongly dominated by GCMs. The same observation holds also for Region D. In general,  
343 regional processes continue to dominate contributions to variability during Oct-Nov, while large scale features  
344 dominate during Dec-Mar.

345

### 346 **3 Discussion and conclusions**

347 In this work we investigated whether it is the RCMs or the driving GCMs that control the monthly precipitation  
348 variability, monthly precipitation biases and the climate change signal over southern Africa and how these  
349 relationships vary from month-to-month through the rainy season. Towards this end, we use an ensemble of 19 RCM  
350 simulations performed in the context of CORDEX-Africa and their driving GCMs. According to the literature  
351 (Munday and Washington, 2018), precipitation in the CMIP5 simulations is characterized by a systematic wet bias  
352 over southern Africa. In the CORDEX-Africa RCM simulations there is also a persistent wet bias, especially during  
353 the core of the rainy season (DJF), however, it is of smaller magnitude and of smaller spatial extent in the RCMs than  
354 the GCMs. It is found that all RCMs reduce monthly precipitation compared to their driving GCMs for both historical  
355 (1985-2005) and future period (2065-2095) under RCP8.5.

356 Over Region B, which encompasses Angola Low (AL) activity, the months with the largest biases are found to be  
357 November and March. November is the month during which there is a transition of the AL from a heat low phase to  
358 a tropical low system, and March indicates the end of the rainy season. Hence, precipitation during the transition  
359 months is challenging for both RCMs and GCMs. Over Region C, representing the wider area of Mozambique, the  
360 bias signal is reversed and after January most of the models display a dry bias. Over South Africa (Region D), the  
361 majority of models display a consistent wet bias for all months of the rainy season. All models (CMIP5 and CORDEX-  
362 Africa) display an intense dry bias in the NE part of SAF, which can be related to the misrepresentation of the moisture  
363 transport entering the region from the Indian Ocean (Munday and Washington, 2018). In general, although RCMs  
364 display an improvement of precipitation biases relative to their driving GCMs, still some bias patterns persist even in  
365 RCMs, calling for a process-based evaluation of specific climatological features such as the formulation of the Angola  
366 Low and the transport of moisture from the NE part of SAF towards central SAF.

367 More specifically, we found that CCLM4-7-18.v1 produces the smallest bias when the whole of SAF is examined,  
368 however, it displays a systematic dry bias over Region C (greater Mozambique region), hence, CCLM4-7-18.v1  
369 should be used with caution over eastern SAF, especially if it is exploited within drought-related climate services.  
370 Concerning RCA4.v1, we find a very regionally heterogeneous -almost pixelated- spatial pattern for precipitation,



371 which can be attributed to the sharp topography used (Van Vooren et al., 2019). RCA4.v1, due to the large size of its  
372 ensemble, is optimal for analyzing its behavior under different driving GCMs. In general, we find that RCA4.v1 is  
373 more prone to follow the signal received from the driving GCMs, contrary to what is observed for CCLM4-7-18.v1.  
374 REMO2009.v1 presents a compromise between the behaviors of RCA4.v1 and CCLM4-7-18.v1.  
375 It is highly recommended that when RCM simulations are used for the whole of SAF or a subregion thereof, the spread  
376 and statistical properties of all available RCMs and their driving GCMs should be examined and an ensemble of RCMs  
377 should be employed based on their ability to reproduce key climatic features of the region of interest. Increasing  
378 evidence is provided that not all models are fit for constructing an ensemble mean (or median) for all regions (Her et  
379 al., 2019; Raju and Kumar, 2020; Tebaldi and Knutti, 2007). Lastly, a very important aspect when the calculation and  
380 characterization of biases is discussed for GCMs and RCMs, is that biases are assessed based on a satellite or gauge-  
381 based product, which are often erroneously regarded as “the ground truth” (Harrison et al., 2019; Alexander et al.,  
382 2020). Of course, the climate community is bound to work with the state-of-the-science products that are available,  
383 however, biases and errors in the “observational datasets” should be kept in sight when the bias of climate models is  
384 discussed. In this work we use the CHIRPS precipitation product, as it has been shown to outperform other satellite  
385 precipitation products (Toté et al., 2015; Ayehu et al., 2018; Dinku et al., 2018).

386  
387 Concerning the climate change signal, there is a strong agreement among all GCMs and RCMs that precipitation  
388 during October will decrease by  $(-0.1) - (-1)$  mm/d, a fact which is associated with a projected later onset of the rainy  
389 season, which is further associated by a northward shift of the tropical rain belt (Dunning et al., 2018). For the rest of  
390 the months, the results are variable, indicating the need for a multi-model approach, when climate change impacts are  
391 assessed. A feature that is identified in some GCMs and is transferred to the downscaling RCMs, is a precipitation  
392 increase that extends from the central SAF region towards the southeast. This result is consistent with previous work  
393 that shows an increase in frequency of landfalling cyclones along the eastern seaboard of SAF (Muthige et al., 2018).  
394 Since tropical cyclones are a particular cause of severe flooding events over the region of Mozambique, there is an  
395 urgent need for planning and mitigation strategies over the region.

396 Lastly, concerning precipitation variability and whether it is the RCMs or the driving GCMs that dominate monthly  
397 precipitation, we find that, as expected, over the whole of SAF (Region A), October and November are dominated by  
398 RCMs, while during Dec-Mar it is the GCMs that mainly formulate the precipitation climatologies. This is explained  
399 by the fact that after December there is a strong large-scale forcing, which is provided to the RCMs by the lateral  
400 boundary conditions given through the GCMs. The results for the historical period are comparable to that for future  
401 projections.

#### 402 *Code and data availability*

403 For the data processing and statistical analysis we used the R Project for Statistical Computing ([https://www.r-](https://www.r-project.org/)  
404 [project.org/](https://www.r-project.org/)), the Climate Data Operators (CDO) (<https://code.mpimet.mpg.de/projects/cdo/>) and Bash programming  
405 routines. Processing scripts are available via ZENODO under DOI: <https://doi.org/10.5281/zenodo.5569984>. CMIP5  
406 and CORDEX-Africa precipitation data were retrieved from the Earth System Grid Federation (ESGF) portal



407 (<https://esgf-data.dkrz.de/projects/esgf-dkrz/>). The Climate Hazards Group InfraRed Precipitation with Station data  
408 (CHIRPS) products were retrieved from: <https://www.chc.ucsb.edu/data/chirps>.

409

410 *Supplement*

411 The supplement related to this article is available online.

412

413 *Author contribution*

414 MCK, SPS and EK designed the research. MCK performed the analysis and prepared the manuscript. SPS, EK, LS  
415 and GN edited the manuscript and provided corrections.

416

417 *Competing interests*

418 The authors declare that they have no competing interests.

419

420 *Acknowledgements*

421 This article is funded by the AfriCultuReS project "Enhancing Food Security in African Agricultural Systems with  
422 the Support of Remote Sensing", (European Union's Horizon 2020 Research and Innovation Framework Programme  
423 under grant agreement No. 774652). The authors would like to thank the Scientific Support Centre of the Aristotle  
424 University of Thessaloniki (Greece) for providing computational/storage infrastructure and technical support. MCK  
425 was funded by the Hellenic Foundation for Research & Innovations, under the 2<sup>nd</sup> Call for PhD Candidates (application  
426 No. 1323).

427

428

429

430

431

432

433

434

435

436

437

438

439



## 440 References

- 441 Abiodun, B.J., Makhanya, N., Petja, B., Abatan, A.A., Oguntunde, P.G., 2019. Future projection of droughts over major river  
442 basins in Southern Africa at specific global warming levels. *Theor. Appl. Climatol.* 137, 1785–1799.  
443 <https://doi.org/10.1007/s00704-018-2693-0>
- 444 Alexander, L.V., Bador, M., Roca, R., Contractor, S., Donat, M.G., Nguyen, P.L., 2020. Intercomparison of annual precipitation  
445 indices and extremes over global land areas from in situ, space-based and reanalysis products. *Environ. Res. Lett.* 15,  
446 055002. <https://doi.org/10.1088/1748-9326/ab79e2>
- 447 Bentsen, M., Bethke, I., Debernard, J.B., Iversen, T., Kirkevåg, A., Seland, Ø., Drange, H., Roelandt, C., Seierstad, I.A., Hoose,  
448 C., Kristjánsson, J.E., 2013. The Norwegian Earth System Model, NorESM1-M – Part 1: Description and basic evaluation  
449 of the physical climate. *Geosci. Model Dev.* 6, 687–720. <https://doi.org/10.5194/gmd-6-687-2013>
- 450 Boberg, F., Christensen, J.H., 2012. Overestimation of Mediterranean summer temperature projections due to model deficiencies.  
451 *Nat. Clim. Change* 2, 433–436. <https://doi.org/10.1038/nclimate1454>
- 452 Casale, M., Dirmie, S., Quinlan, T., Ziervogel, G., 2010. Understanding vulnerability in southern Africa: comparative findings  
453 using a multiple-stressor approach in South Africa and Malawi. *Reg. Environ. Change* 10, 157–168.  
454 <https://doi.org/10.1007/s10113-009-0103-y>
- 455 CCCma, 2017. Environment and Climate Change Canada - Climate Change - CanESM2 [WWW Document]. URL  
456 <http://www.ec.gc.ca/ccmac-cccma/default.asp?lang=En&xml=1A3B7DF1-99BB-4EC8-B129-09F83E72D645>  
457 (accessed 6.23.20).
- 458 Christensen, O.B., Kjellström, E., 2020. Partitioning uncertainty components of mean climate and climate change in a large  
459 ensemble of European regional climate model projections. *Clim. Dyn.* 54, 4293–4308. [https://doi.org/10.1007/s00382-](https://doi.org/10.1007/s00382-020-05229-y)  
460 [020-05229-y](https://doi.org/10.1007/s00382-020-05229-y)
- 461 Collins, W.J., Bellouin, N., Doutriaux-Boucher, M., Gedney, N., Halloran, P., Hinton, T., Hughes, J., Jones, C.D., Joshi, M.,  
462 Liddicoat, S., Martin, G., O'Connor, F., Rae, J., Senior, C., Sitch, S., Totterdell, I., Wiltshire, A., Woodward, S., 2011.  
463 Development and evaluation of an Earth-System model – HadGEM2. *Geosci. Model Dev.* 4, 1051–1075.  
464 <https://doi.org/10.5194/gmd-4-1051-2011>
- 465 Conway, D., van Garderen, E.A., Deryng, D., Dorling, S., Krueger, T., Landman, W., Lankford, B., Lebek, K., Osborn, T., Ringer,  
466 C., Thurlow, J., Zhu, T., Dalin, C., 2015. Climate and southern Africa's water–energy–food nexus. *Nat. Clim. Change* 5,  
467 837–846. <https://doi.org/10.1038/nclimate2735>
- 468 Crétaut, J., Pohl, B., Dieppois, B., Berthou, S., Pergaud, J., 2019. The Angola Low: relationship with southern African rainfall and  
469 ENSO. *Clim. Dyn.* 52, 1783–1803. <https://doi.org/10.1007/s00382-018-4222-3>
- 470 Déqué, M., Rowell, D.P., Lüthi, D., Giorgi, F., Christensen, J.H., Rockel, B., Jacob, D., Kjellström, E., de Castro, M., van den  
471 Hurk, B., 2007. An intercomparison of regional climate simulations for Europe: assessing uncertainties in model  
472 projections. *Clim. Change* 81, 53–70. <https://doi.org/10.1007/s10584-006-9228-x>
- 473 Déqué, M., Somot, S., Sanchez-Gomez, E., Goodess, C.M., Jacob, D., Lenderink, G., Christensen, O.B., 2012. The spread amongst  
474 ENSEMBLES regional scenarios: regional climate models, driving general circulation models and interannual  
475 variability. *Clim. Dyn.* 38, 951–964. <https://doi.org/10.1007/s00382-011-1053-x>
- 476 Dinku, T., Funk, C., Peterson, P., Maidment, R., Tadesse, T., Gadain, H., Ceccato, P., 2018. Validation of the CHIRPS satellite  
477 rainfall estimates over eastern Africa. *Q. J. R. Meteorol. Soc.* 144, 292–312. <https://doi.org/10.1002/qj.3244>
- 478 Di Luca, A., de Elfa, R., Laprise, R., 2013. Potential for added value in temperature simulated by high-resolution nested RCMs in  
479 present climate and in the climate change signal. *Clim. Dyn.* 40, 443–464. <https://doi.org/10.1007/s00382-012-1384-2>
- 480 Diffenbaugh, N.S., Giorgi, F., 2012. Climate change hotspots in the CMIP5 global climate model ensemble. *Clim. Change* 114,  
481 813–822. <https://doi.org/10.1007/s10584-012-0570-x>
- 482 Dosio, A., Jones, R.G., Jack, C., Lennard, C., Nikulin, G., Hewitson, B., 2019. What can we know about future precipitation in  
483 Africa? Robustness, significance and added value of projections from a large ensemble of regional climate models. *Clim.*  
484 *Dyn.* 53, 5833–5858. <https://doi.org/10.1007/s00382-019-04900-3>
- 485 Dufresne, J.-L., Foujols, M.-A., Denvil, S., Caubel, A., Marti, O., Aumont, O., Balkanski, Y., Bekki, S., Bellenger, H., Benshila,  
486 R., Bony, S., Bopp, L., Braconnot, P., Brockmann, P., Cadule, P., Cheruy, F., Codron, F., Cozic, A., Cugnet, D., de  
487 Noblet, N., Duvel, J.-P., Ethé, C., Fairhead, L., Fichefet, T., Flavoni, S., Friedlingstein, P., Grandpeix, J.-Y., Guez, L.,  
488 Guilyardi, E., Hauglustaine, D., Hourdin, F., Idelkadi, A., Ghattas, J., Joussaume, S., Kageyama, M., Krinner, G.,  
489 Labetoulle, S., Lahellec, A., Lefebvre, M.-P., Lefebvre, F., Levy, C., Li, Z.X., Lloyd, J., Lott, F., Madec, G., Mancip, M.,  
490 Marchand, M., Masson, S., Meurdesoif, Y., Mignot, J., Musat, I., Parouty, S., Polcher, J., Rio, C., Schulz, M.,  
491 Swingedouw, D., Szopa, S., Talandier, C., Terray, P., Viovy, N., Vuichard, N., 2013. Climate change projections using  
492 the IPSL-CM5 Earth System Model: from CMIP3 to CMIP5. *Clim. Dyn.* 40, 2123–2165. [https://doi.org/10.1007/s00382-](https://doi.org/10.1007/s00382-012-1636-1)  
493 [012-1636-1](https://doi.org/10.1007/s00382-012-1636-1)
- 494 Dunne, J.P., John, J.G., Adcroft, A.J., Griffies, S.M., Hallberg, R.W., Shevliakova, E., Stouffer, R.J., Cooke, W., Dunne, K.A.,  
495 Harrison, M.J., Krasting, J.P., Malyshev, S.L., Milly, P.C.D., Philipps, P.J., Sentman, L.T., Samuels, B.L., Spelman,  
496 M.J., Winton, M., Wittenberg, A.T., Zadeh, N., 2012. GFDL's ESM2 Global Coupled Climate–Carbon Earth System  
497 Models. Part I: Physical Formulation and Baseline Simulation Characteristics. *J. Clim.* 25, 6646–6665.  
498 <https://doi.org/10.1175/JCLI-D-11-00560.1>
- 499 Dunning, C.M., Black, E., Allan, R.P., 2018. Later Wet Seasons with More Intense Rainfall over Africa under Future Climate  
500 Change. *J. Clim.* 31, 9719–9738. <https://doi.org/10.1175/JCLI-D-18-0102.1>



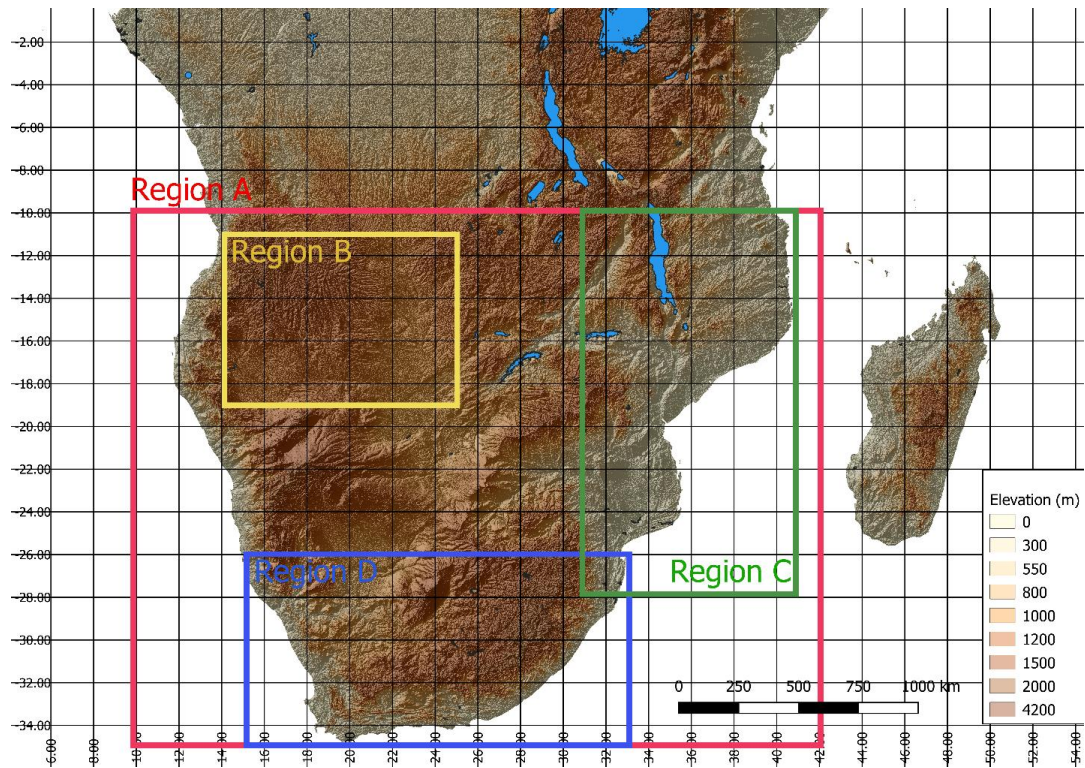
- 501 Funk, C., Peterson, P., Landsfeld, M., Pedreros, D., Verdin, J., Shukla, S., Husak, G., Rowland, J., Harrison, L., Hoell, A.,  
502 Michaelsen, J., 2015. The climate hazards infrared precipitation with stations—a new environmental record for  
503 monitoring extremes. *Sci. Data* 2, 150066. <https://doi.org/10.1038/sdata.2015.66>
- 504 Giorgetta, M.A., Jungclaus, J., Reick, C.H., Legutke, S., Bader, J., Böttinger, M., Brovkin, V., Crueger, T., Esch, M., Fieg, K.,  
505 Glushak, K., Gayler, V., Haak, H., Hollweg, H.-D., Ilyina, T., Kinne, S., Kornblueh, L., Matei, D., Mauritsen, T.,  
506 Mikolajewicz, U., Mueller, W., Notz, D., Pithan, F., Raddatz, T., Rast, S., Redler, R., Roeckner, E., Schmidt, H., Schnur,  
507 R., Segsneider, J., Six, K.D., Stockhause, M., Timmreck, C., Wegner, J., Widmann, H., Wieners, K.-H., Claussen, M.,  
508 Marotzke, J., Stevens, B., 2013. Climate and carbon cycle changes from 1850 to 2100 in MPI-ESM simulations for the  
509 Coupled Model Intercomparison Project phase 5. *J. Adv. Model. Earth Syst.* 5, 572–597.  
510 <https://doi.org/10.1002/jame.20038>
- 511 Giorgi, F., Gutowski, W.J., 2015. Regional Dynamical Downscaling and the CORDEX Initiative. *Annu. Rev. Environ. Resour.* 40,  
512 467–490. <https://doi.org/10.1146/annurev-environ-102014-021217>
- 513 Harrison, L., Funk, C., Peterson, P., 2019. Identifying changing precipitation extremes in Sub-Saharan Africa with gauge and  
514 satellite products. *Environ. Res. Lett.* 14, 085007. <https://doi.org/10.1088/1748-9326/ab2cae>
- 515 Hazeleger, W., Severijns, C., Semmler, T., Ștefănescu, S., Yang, S., Wang, X., Wyser, K., Dutra, E., Baldasano, J.M., Bintanja,  
516 R., Bougeault, P., Caballero, R., Ekman, A.M.L., Christensen, J.H., van den Hurk, B., Jimenez, P., Jones, C., Källberg,  
517 P., Koenigk, T., McGrath, R., Miranda, P., van Noije, T., Palmer, T., Parodi, J.A., Schmith, T., Seltén, F., Storelvmo, T.,  
518 Sterl, A., Tapamo, H., Vancoppenolle, M., Viterbo, P., Willén, U., 2010. EC-EarthA Seamless Earth-System Prediction  
519 Approach in Action. *Bull. Am. Meteorol. Soc.* 91, 1357–1364. <https://doi.org/10.1175/2010BAMS2877.1>
- 520 Her, Y., Yoo, S.-H., Cho, J., Hwang, S., Jeong, J., Seong, C., 2019. Uncertainty in hydrological analysis of climate change: multi-  
521 parameter vs. multi-GCM ensemble predictions. *Sci. Rep.* 9, 4974. <https://doi.org/10.1038/s41598-019-41334-7>
- 522 Howard, E., Washington, R., 2018. Characterizing the Synoptic Expression of the Angola Low. *J. Clim.* 31, 7147–7165.  
523 <https://doi.org/10.1175/JCLI-D-18-0017.1>
- 524 IPCC, Stocker, T.F., 2013. *Climate Change 2013: The Physical Science Basis*. Cambridge University Press.
- 525 Jeffrey, S., Rotstayn, L.D., Collier, M., Dravitzki, S.M., Hamalainen, C., Moeseneder, C., Wong, K., Syktus, J., 2013. Australia 's  
526 CMIP 5 submission using the CSIRO-Mk 3. 6 model.
- 527 Kerkhoff, C., Künsch, H.R., Schär, C., 2015. A Bayesian Hierarchical Model for Heterogeneous RCM–GCM Multimodel  
528 Ensembles. *J. Clim.* 28, 6249–6266. <https://doi.org/10.1175/JCLI-D-14-00606.1>
- 529 Lima, D.C.A., Soares, P.M.M., Semedo, A., Cardoso, R.M., Cabos, W., Sein, D.V., 2019. How Will a Warming Climate Affect  
530 the Benguela Coastal Low-Level Wind Jet? *J. Geophys. Res. Atmospheres* 124, 5010–5028.  
531 <https://doi.org/10.1029/2018JD029574>
- 532 Luan, Y., Cui, X., Ferrat, M., 2013. Historical trends of food self-sufficiency in Africa. *Food Secur.* 5, 393–405.  
533 <https://doi.org/10.1007/s12571-013-0260-1>
- 534 Lyon, B., Mason, S.J., 2007. The 1997–98 Summer Rainfall Season in Southern Africa. Part I: Observations. *J. Clim.* 20, 5134–  
535 5148. <https://doi.org/10.1175/JCLI4225.1>
- 536 Masipa, T.S., 2017. The impact of climate change on food security in South Africa: Current realities and challenges ahead. *Jamba*  
537 *J. Disaster Risk Stud.* 9. <https://doi.org/10.4102/jamba.v9i1.411>
- 538 Maúre, G., Pinto, I., Ndebele-Murisa, M., Muthige, M., Lennard, C., Nikulin, G., Dosio, A., Meque, A., 2018. The southern African  
539 climate under 1.5\hpace0.167em°C and 2\hpace0.167em°C of global warming as simulated by CORDEX regional  
540 climate models. *Environ. Res. Lett.* 13, 065002. <https://doi.org/10.1088/1748-9326/aab190>
- 541 Misselhorn, A., Hendriks, S.L., 2017. A systematic review of sub-national food insecurity research in South Africa: Missed  
542 opportunities for policy insights. *PLOS ONE* 12, e0182399. <https://doi.org/10.1371/journal.pone.0182399>
- 543 Munday, C., Washington, R., 2018. Systematic Climate Model Rainfall Biases over Southern Africa: Links to Moisture Circulation  
544 and Topography. *J. Clim.* 31, 7533–7548. <https://doi.org/10.1175/JCLI-D-18-0008.1>
- 545 Munday, C., Washington, R., 2017. Circulation controls on southern African precipitation in coupled models: The role of the  
546 Angola Low. *J. Geophys. Res. Atmospheres* 122, 861–877. <https://doi.org/10.1002/2016JD025736>
- 547 Muthige, M.S., Malherbe, J., Englebrecht, F.A., Grab, S., Beraki, A., Maisha, T.R., Merwe, J.V. der, 2018. Projected changes in  
548 tropical cyclones over the South West Indian Ocean under different extents of global warming. *Environ. Res. Lett.* 13,  
549 065019. <https://doi.org/10.1088/1748-9326/aab60>
- 550 Nicholson, S.E., 2018. The ITCZ and the Seasonal Cycle over Equatorial Africa. *Bull. Am. Meteorol. Soc.* 99, 337–348.  
551 <https://doi.org/10.1175/BAMS-D-16-0287.1>
- 552 Nikulin, G., Jones, C., Giorgi, F., Asrar, G., Büchner, M., Cerezo-Mota, R., Christensen, O.B., Déqué, M., Fernandez, J., Hänsler,  
553 A., van Meijgaard, E., Samuelsson, P., Sylla, M.B., Sushama, L., 2012. Precipitation Climatology in an Ensemble of  
554 CORDEX-Africa Regional Climate Simulations. *J. Clim.* 25, 6057–6078. <https://doi.org/10.1175/JCLI-D-11-00375.1>
- 555 Pinto, I., Jack, C., Hewitson, B., 2018. Process-based model evaluation and projections over southern Africa from Coordinated  
556 Regional Climate Downscaling Experiment and Coupled Model Intercomparison Project Phase 5 models. *Int. J. Climatol.*  
557 38, 4251–4261. <https://doi.org/10.1002/joc.5666>
- 558 Pinto, I., Lennard, C., Tadross, M., Hewitson, B., Dosio, A., Nikulin, G., Panitz, H.-J., Shongwe, M.E., 2016. Evaluation and  
559 projections of extreme precipitation over southern Africa from two CORDEX models. *Clim. Change* 135, 655–668.  
560 <https://doi.org/10.1007/s10584-015-1573-1>
- 561 Raju, K.S., Kumar, D.N., 2020. Review of approaches for selection and ensembling of GCMs. *J. Water Clim. Change* 11, 577–  
562 599. <https://doi.org/10.2166/wcc.2020.128>



- 563 Reason, C.J.C., Jagadheesha, D., 2005. A model investigation of recent ENSO impacts over southern Africa. *Meteorol.*  
564 *Atmospheric Phys.* 89, 181–205. <https://doi.org/10.1007/s00703-005-0128-9>
- 565 Reboita, M.S., Ambrizzi, T., Silva, B.A., Pinheiro, R.F., da Rocha, R.P., 2019. The South Atlantic Subtropical Anticyclone: Present  
566 and Future Climate. *Front. Earth Sci.* 0. <https://doi.org/10.3389/feart.2019.00008>
- 567 Shew, A.M., Tack, J.B., Nalley, L.L., Chaminuka, P., 2020. Yield reduction under climate warming varies among wheat cultivars  
568 in South Africa. *Nat. Commun.* 11, 4408. <https://doi.org/10.1038/s41467-020-18317-8>
- 569 Sillmann, J., Kharin, V.V., Zwiers, F.W., Zhang, X., Bronaugh, D., 2013. Climate extremes indices in the CMIP5 multimodel  
570 ensemble: Part 2. Future climate projections. *J. Geophys. Res. Atmospheres* 118, 2473–2493.  
571 <https://doi.org/10.1002/jgrd.50188>
- 572 Sørland, S.L., Schär, C., Lüthi, D., Kjellström, E., 2018. Bias patterns and climate change signals in GCM-RCM model chains.  
573 *Environ. Res. Lett.* 13, 074017. <https://doi.org/10.1088/1748-9326/aacc77>
- 574 Taylor, K.E., Stouffer, R.J., Meehl, G.A., 2012. An Overview of CMIP5 and the Experiment Design. *Bull. Am. Meteorol. Soc.* 93,  
575 485–498. <https://doi.org/10.1175/BAMS-D-11-00094.1>
- 576 Tebaldi, C., Knutti, R., 2007. The use of the multi-model ensemble in probabilistic climate projections. *Philos. Trans. R. Soc. Math.*  
577 *Phys. Eng. Sci.* 365, 2053–2075. <https://doi.org/10.1098/rsta.2007.2076>
- 578 Vautard, R., Kadyrov, N., Iles, C., Boberg, F., Buonomo, E., Bülow, K., Coppola, E., Corre, L., Meijgaard, E. van, Nogherotto,  
579 R., Sandstad, M., Schwingshackl, C., Somot, S., Aalbers, E., Christensen, O.B., Ciarlò, J.M., Demory, M.-E., Giorgi, F.,  
580 Jacob, D., Jones, R.G., Keuler, K., Kjellström, E., Lenderink, G., Levvasseur, G., Nikulin, G., Sillmann, J., Solidoro,  
581 C., Sørland, S.L., Steger, C., Teichmann, C., Warrach-Sagi, K., Wulfmeyer, V., 2020. Evaluation of the large EURO-  
582 CORDEX regional climate model ensemble. *J. Geophys. Res. Atmospheres* n/a, e2019JD032344.  
583 <https://doi.org/10.1029/2019JD032344>
- 584 Voltaire, A., Sanchez-Gomez, E., Salas y Méliá, D., Decharme, B., Cassou, C., Sénési, S., Valcke, S., Beau, I., Alias, A.,  
585 Chevallier, M., Déqué, M., Deshayes, J., Douville, H., Fernandez, E., Madec, G., Maisonnave, E., Moine, M.-P., Planton,  
586 S., Saint-Martin, D., Szopa, S., Tyteca, S., Alkama, R., Belamari, S., Braun, A., Coquart, L., Chauvin, F., 2013. The  
587 CNRM-CM5.1 global climate model: description and basic evaluation. *Clim. Dyn.* 40, 2091–2121.  
588 <https://doi.org/10.1007/s00382-011-1259-y>
- 589 Watanabe, M., Suzuki, T., Oishi, R., Komuro, Y., Watanabe, S., Emori, S., Takemura, T., Chikira, M., Ogura, T., Sekiguchi, M.,  
590 Takata, K., Yamazaki, D., Yokohata, T., Nozawa, T., Hasumi, H., Tatebe, H., Kimoto, M., 2010. Improved Climate  
591 Simulation by MIROC5: Mean States, Variability, and Climate Sensitivity. *J. Clim.* 23, 6312–6335.  
592 <https://doi.org/10.1175/2010JCLI3679.1>
- 593 Wolski, P., Lobell, D., Stone, D., Pinto, I., Crespo, O., Johnston, P., 2020. On the role of anthropogenic climate change in the  
594 emerging food crisis in southern Africa in the 2019–2020 growing season. *Glob. Change Biol.* 26, 2729–2730.  
595 <https://doi.org/10.1111/gcb.15047>
- 596 Wu, J., Gao, X., 2020. Present day bias and future change signal of temperature over China in a series of multi-GCM driven RCM  
597 simulations. *Clim. Dyn.* 54, 1113–1130. <https://doi.org/10.1007/s00382-019-05047-x>
- 598 Gessesse, B., Dinku, T., 2018. Validation of new satellite rainfall products over the Upper Blue Nile Basin, Ethiopia.  
599 *Atmospheric Meas. Tech.* 11, 1921–1936. <https://doi.org/10.5194/amt-11-1921-2018>
- 600 Giorgi, F., Gutowski, W.J., 2015. Regional Dynamical Downscaling and the CORDEX Initiative. *Annu. Rev. Environ. Resour.* 40,  
601 467–490. <https://doi.org/10.1146/annurev-environ-102014-021217>
- 602 Lloyd, E.A., Bukovsky, M., Mearns, L.O., 2020. An analysis of the disagreement about added value by regional climate models.  
603 *Synthese.* <https://doi.org/10.1007/s11229-020-02821-x>
- 604 Luca, A.D., Argüeso, D., Evans, J.P., Elía, R. de, Laprise, R., 2016. Quantifying the overall added value of dynamical downscaling  
605 and the contribution from different spatial scales. *J. Geophys. Res. Atmospheres* 121, 1575–1590.  
606 <https://doi.org/10.1002/2015JD024009>
- 607 Macron, C., Pohl, B., Richard, Y., Bessafi, M., 2014. How do Tropical Temperate Troughs Form and Develop over Southern  
608 Africa? *J. Clim.* 27, 1633–1647. <https://doi.org/10.1175/JCLI-D-13-00175.1>
- 609 Nikulin, G., Jones, C., Giorgi, F., Asrar, G., Büchner, M., Cerezo-Mota, R., Christensen, O.B., Déqué, M., Fernandez, J., Hänsler,  
610 A., van Meijgaard, E., Samuelsson, P., Sylla, M.B., Sushama, L., 2012. Precipitation Climatology in an Ensemble of  
611 CORDEX-Africa Regional Climate Simulations. *J. Clim.* 25, 6057–6078. <https://doi.org/10.1175/JCLI-D-11-00375.1>
- 612 Rana, A., Nikulin, G., Kjellström, E., Strandberg, G., Kupiainen, M., Hansson, U., Kolax, M., 2020. Contrasting regional and  
613 global climate simulations over South Asia. *Clim. Dyn.* 54, 2883–2901. <https://doi.org/10.1007/s00382-020-05146-0>
- 614 Ratna, S.B., Behera, S., Ratnam, J.V., Takahashi, K., Yamagata, T., 2013. An index for tropical temperate troughs over southern  
615 Africa. *Clim. Dyn.* 41, 421–441. <https://doi.org/10.1007/s00382-012-1540-8>
- 616 Shongwe, M.E., Lennard, C., Liebmann, B., Kalognomou, E.-A., Ntsangwane, L., Pinto, I., 2015. An evaluation of CORDEX  
617 regional climate models in simulating precipitation over Southern Africa. *Atmospheric Sci. Lett.* 16, 199–207.  
618 <https://doi.org/10.1002/asl2.538>
- 619 Sørland, S.L., Schär, C., Lüthi, D., Kjellström, E., 2018. Bias patterns and climate change signals in GCM-RCM model chains.  
620 *Environ. Res. Lett.* 13, 074017. <https://doi.org/10.1088/1748-9326/aacc77>
- 621 Toté, C., Patricio, D., Boogaard, H., Van der Wijngaart, R., Tarnavsky, E., Funk, C., 2015. Evaluation of Satellite Rainfall Estimates  
622 for Drought and Flood Monitoring in Mozambique. *Remote Sens.* 7, 1758–1776. <https://doi.org/10.3390/rs70201758>



- 623 Van Vooren, S., Van Schaeybroeck, B., Nyssen, J., Van Ginderachter, M., Termonia, P., 2019. Evaluation of CORDEX rainfall in  
624 northwest Ethiopia: Sensitivity to the model representation of the orography. *Int. J. Climatol.* 39, 2569–2586.  
625 <https://doi.org/10.1002/joc.5971>
- 626 Vautard, R., Kadyrov, N., Iles, C., Boberg, F., Buonomo, E., Bülow, K., Coppola, E., Corre, L., Meijgaard, E. van, Nogherotto,  
627 R., Sandstad, M., Schwingshackl, C., Somot, S., Aalbers, E., Christensen, O.B., Ciarlò, J.M., Demory, M.-E., Giorgi, F.,  
628 Jacob, D., Jones, R.G., Keuler, K., Kjellström, E., Lenderink, G., Levvasseur, G., Nikulin, G., Sillmann, J., Solidoro,  
629 C., Sørland, S.L., Steger, C., Teichmann, C., Warrach-Sagi, K., Wulfmeyer, V., 2020. Evaluation of the large EURO-  
630 CORDEX regional climate model ensemble. *J. Geophys. Res. Atmospheres* n/a, e2019JD032344.  
631 <https://doi.org/10.1029/2019JD032344>
- 632 Wu, J., Gao, X., 2020. Present day bias and future change signal of temperature over China in a series of multi-GCM driven RCM  
633 simulations. *Clim. Dyn.* 54, 1113–1130. <https://doi.org/10.1007/s00382-019-05047-x>  
634  
635
- 636
- 637
- 638
- 639
- 640
- 641
- 642



643

644 **Figure 1.** Study region and subregions over southern Africa.

645

646

647

648

649

650

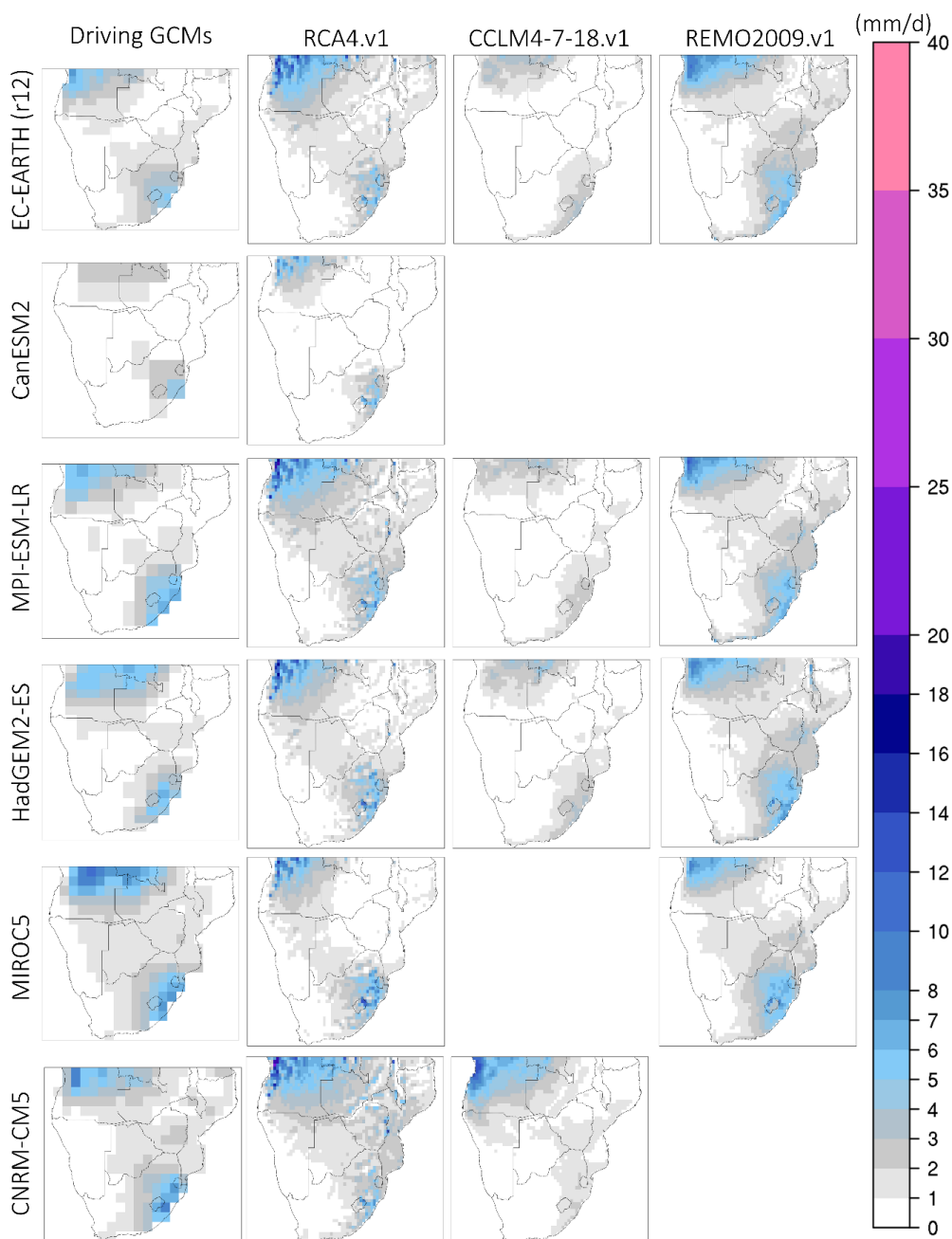
651

652

653

654

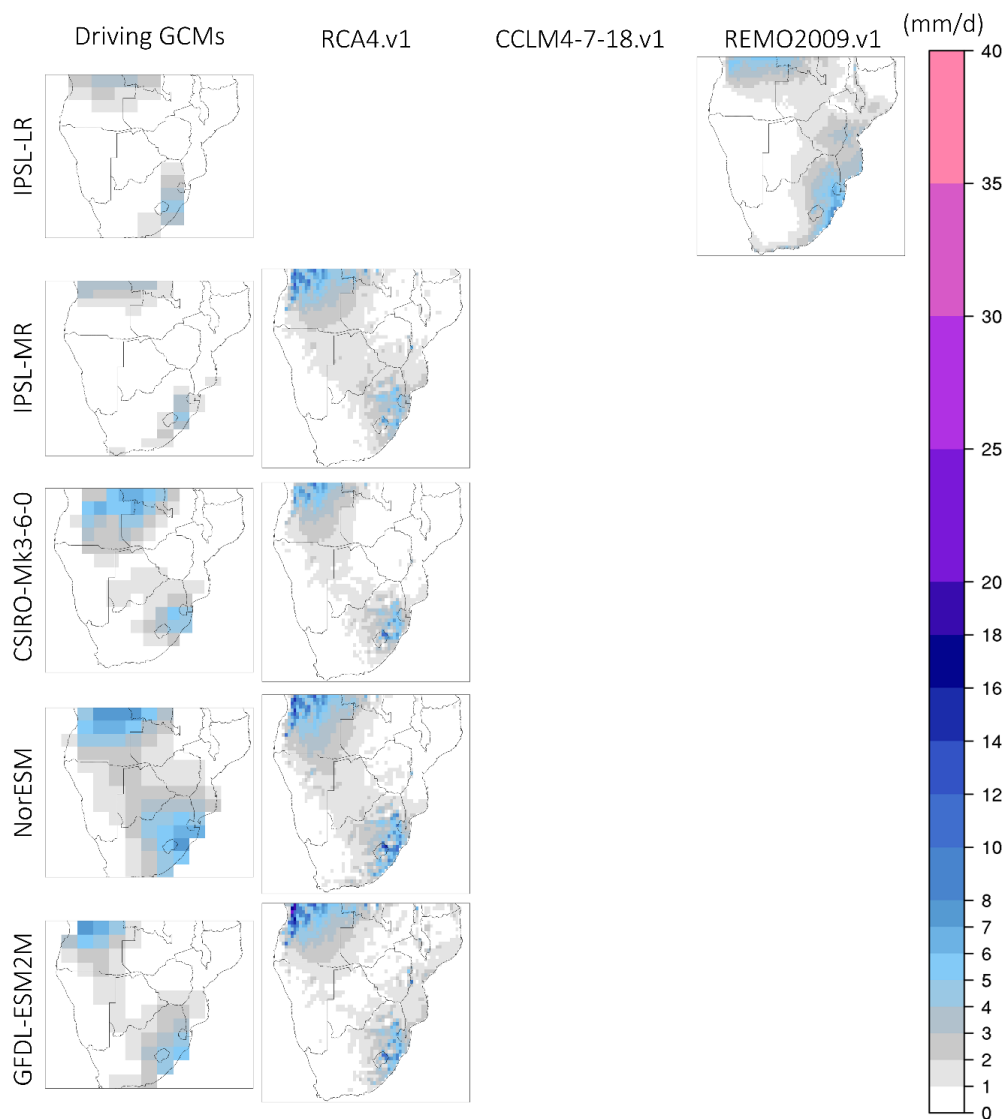
655



656

657 **Figure 2.** Monthly precipitation climatologies (mm/d) during October for the period 1985-2005. First column (from  
658 the left) displays precipitation from the driving GCMs and columns 2-4 display the downscaled precipitation output  
659 from RCA4.v1, CCLM4-8-17.v1 and REMO2009.v1.

660



661

662 **Figure 2.** Continued.

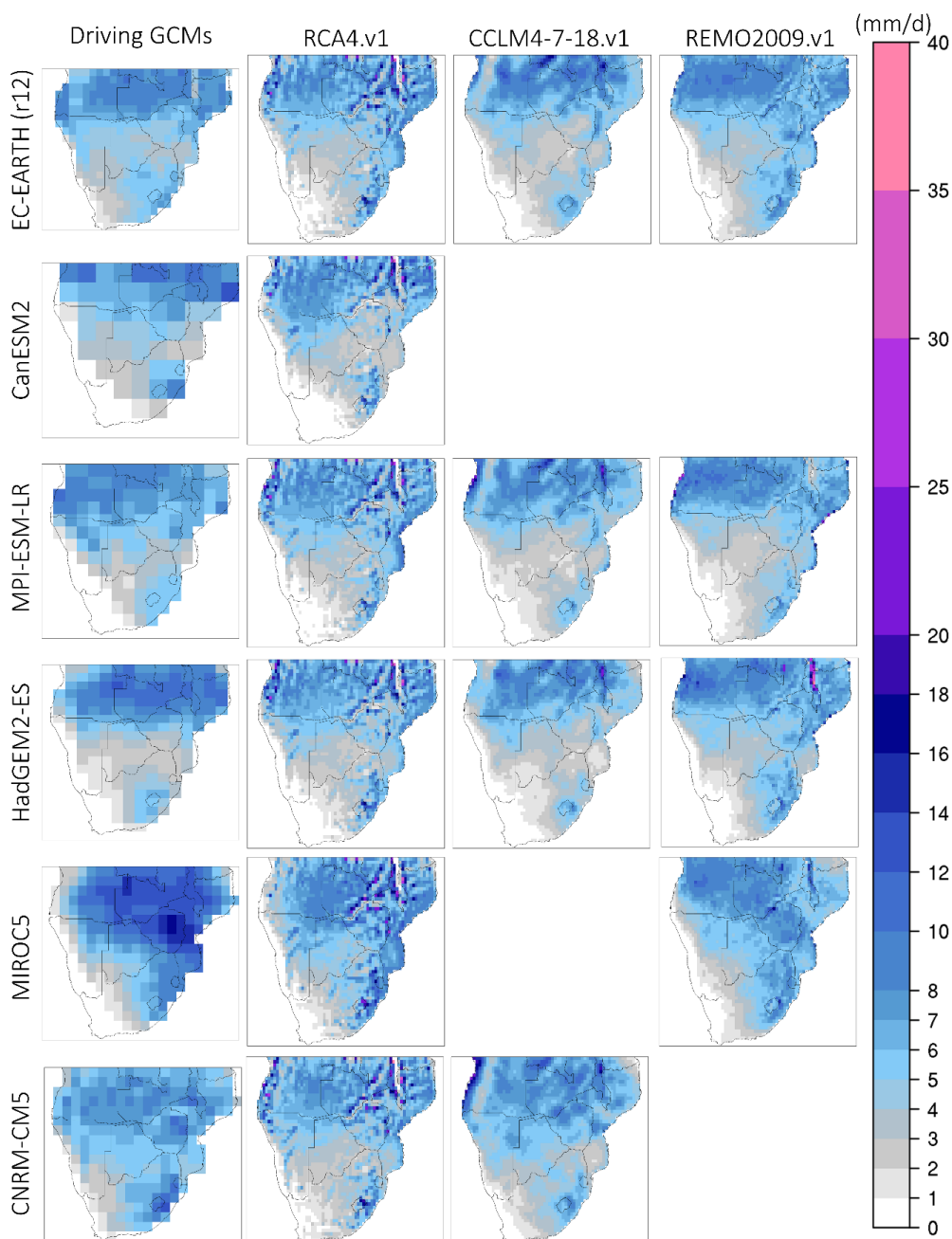
663

664

665

666

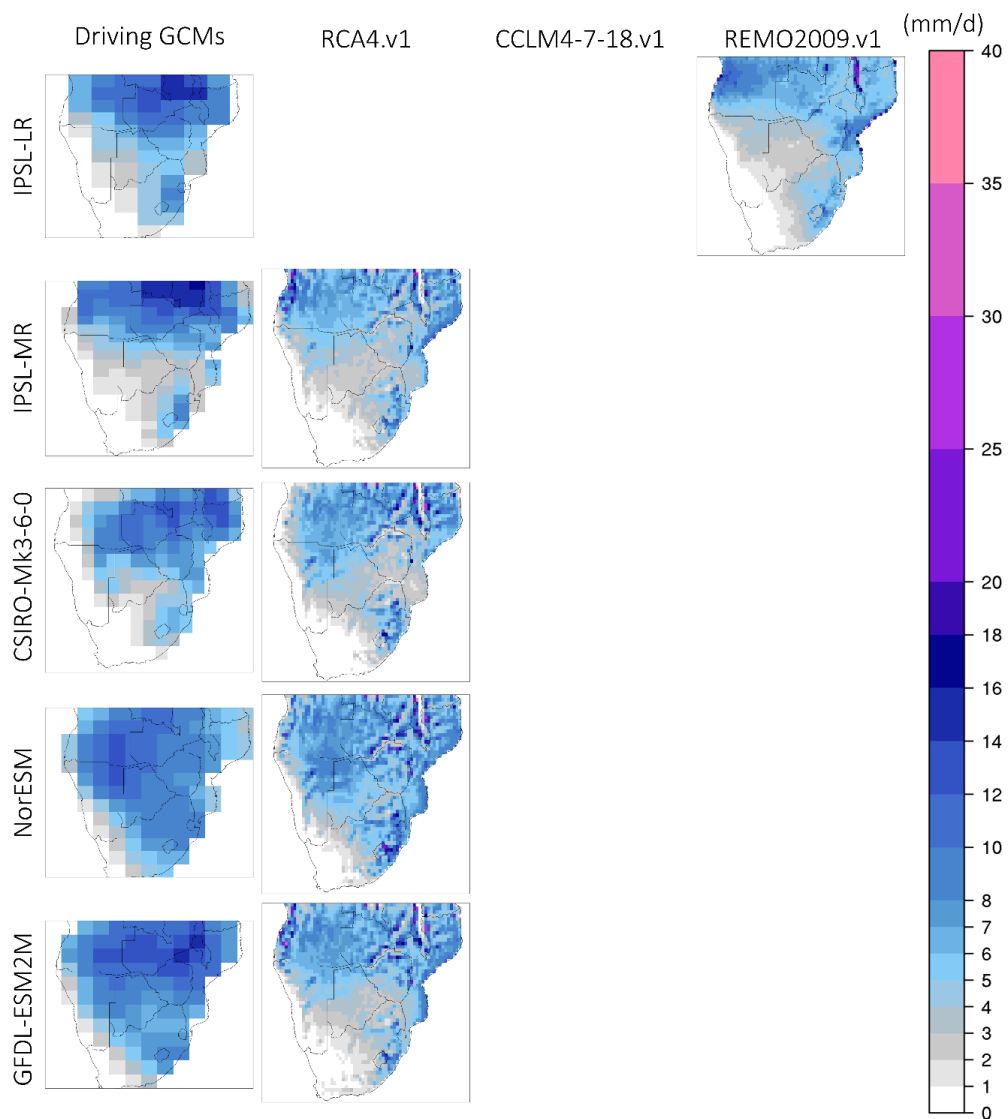
667



668

669 **Figure 3.** Monthly precipitation climatologies (mm/d) during January for the period 1985-2005. First column (from  
670 the left) displays precipitation from the driving GCMs and columns 2-4 display the downscaled precipitation output  
671 from RCA4.v1, CCLM4-8-17.v1 and REMO2009.v1.

672



673

674 **Figure 3.** Continued.

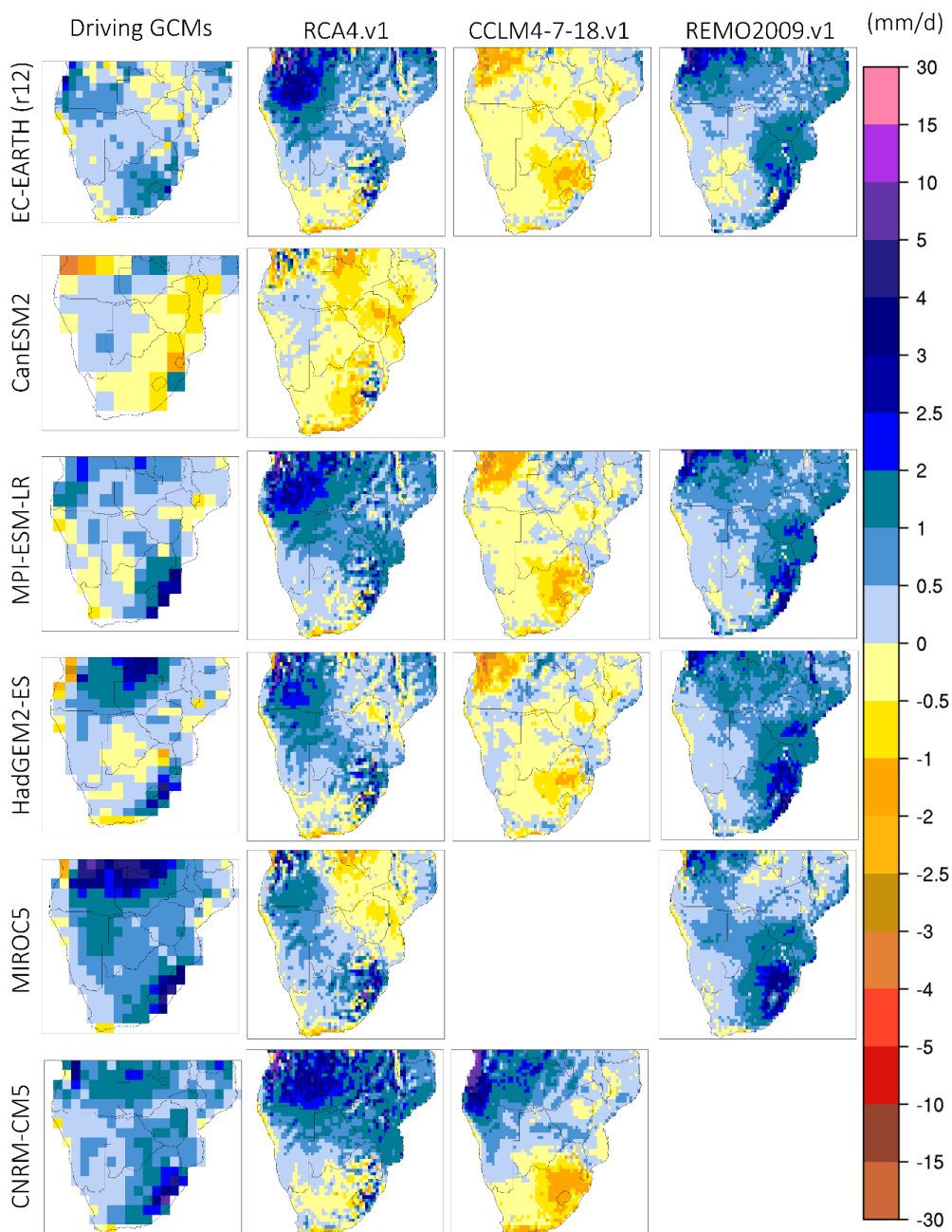
675

676

677

678

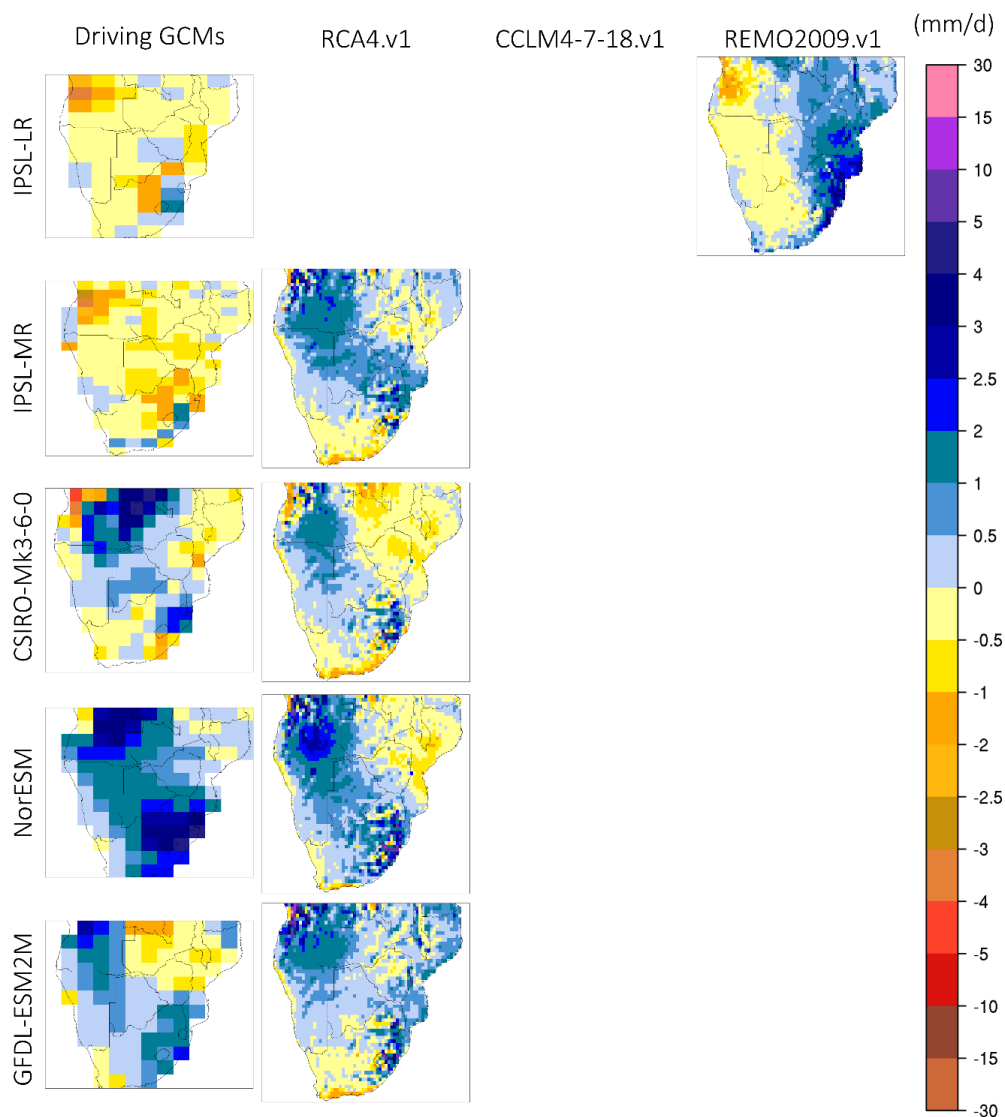
679



680

681 **Figure 4.** Monthly precipitation bias (model – CHIRPS in mm/d) during October for the period 1985-2005. First  
682 column (from the left) displays the biases in the driving GCMs and columns 2-4 display the biases in the downscaled  
683 precipitation output according to RCA4.v1, CCLM4-8-17.v1 and REMO2009.v1.

684



685

686 **Figure 4.** Continued.

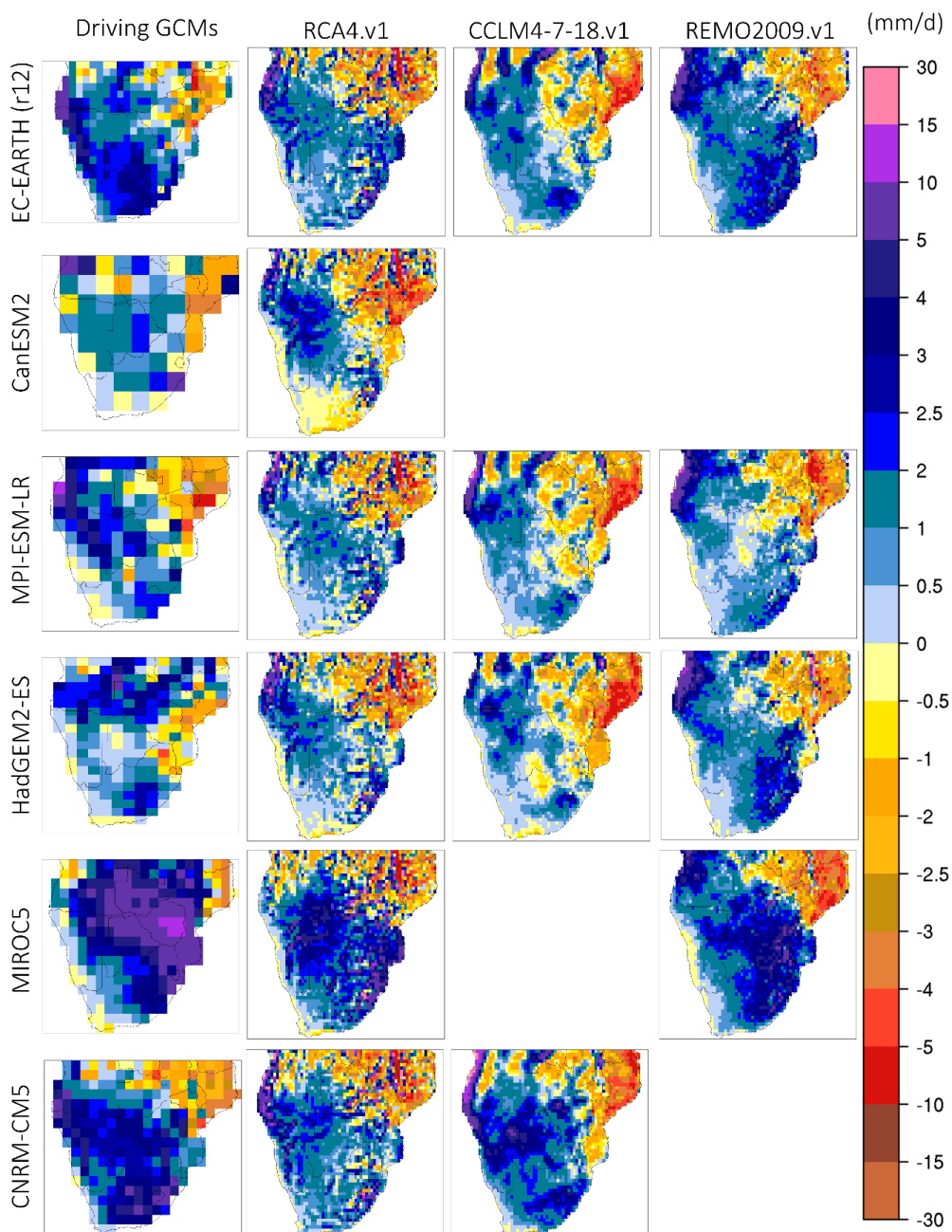
687

688

689

690

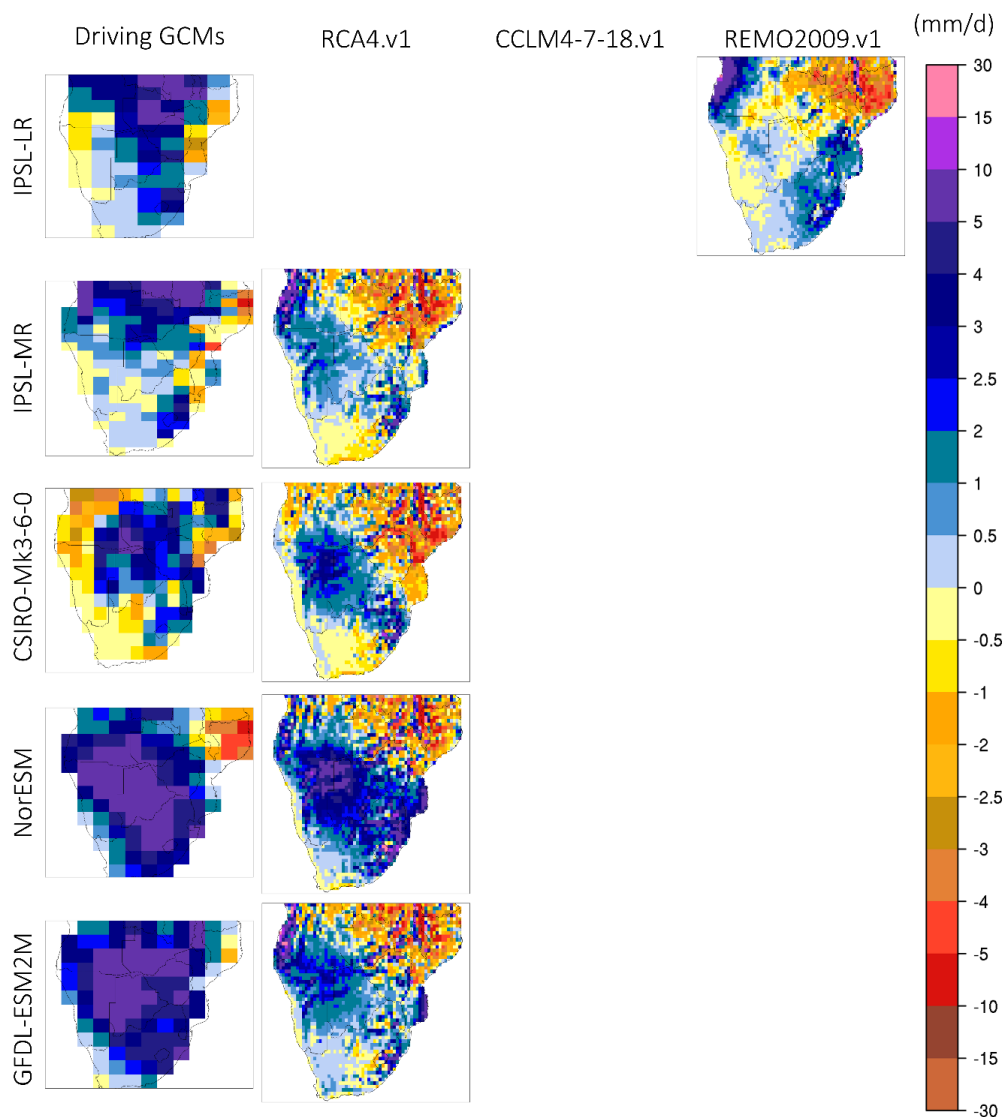
691



692

693 **Figure 5.** Monthly precipitation biases (model – CHIRPS in mm/d) during January for the period 1985-2005. First  
694 column (from the left) displays precipitation biases from the driving GCMs used and columns 2-4 display the  
695 downscaled products according to RCA4.v1, CCLM4-8-17.v1 and REMO2009.v1.

696



697

698 **Figure 5.** Continued.

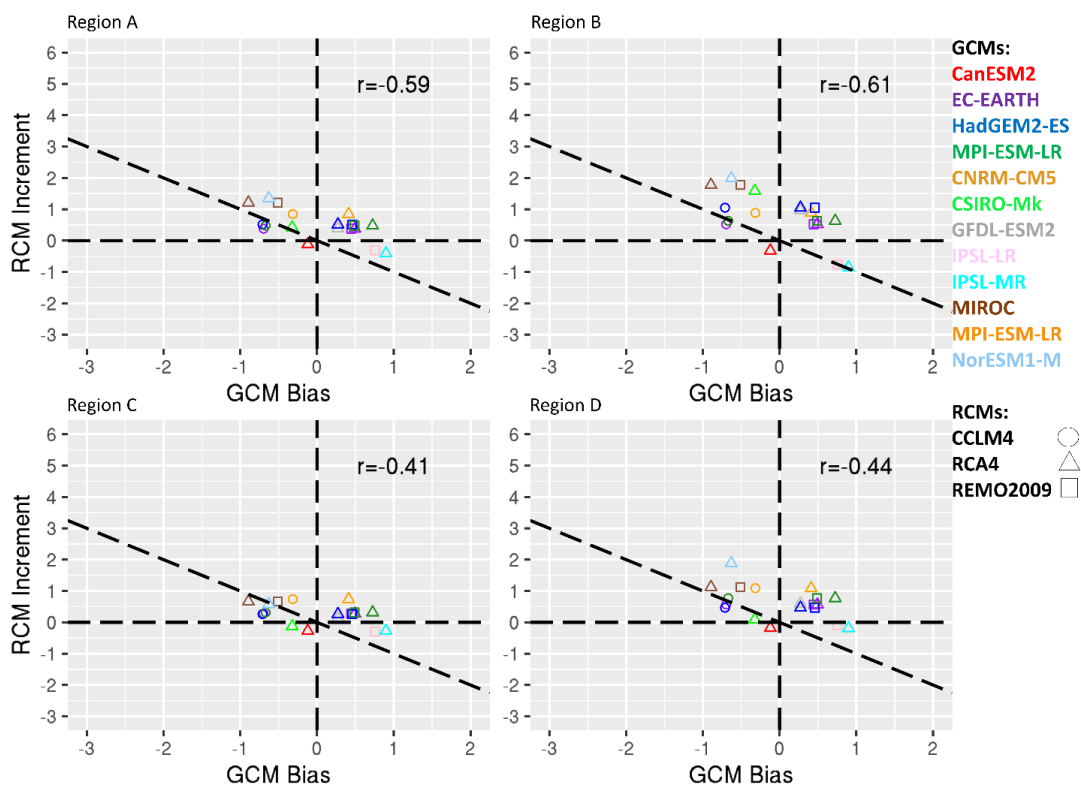
699

700

701

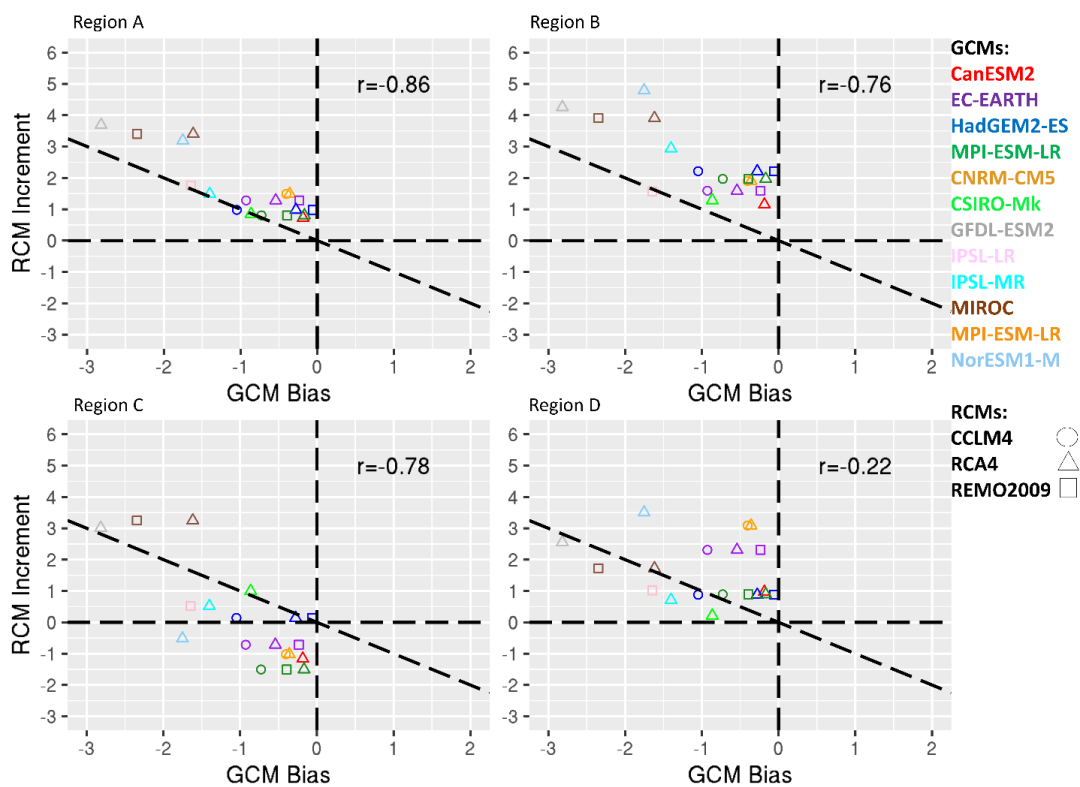
702

703



704

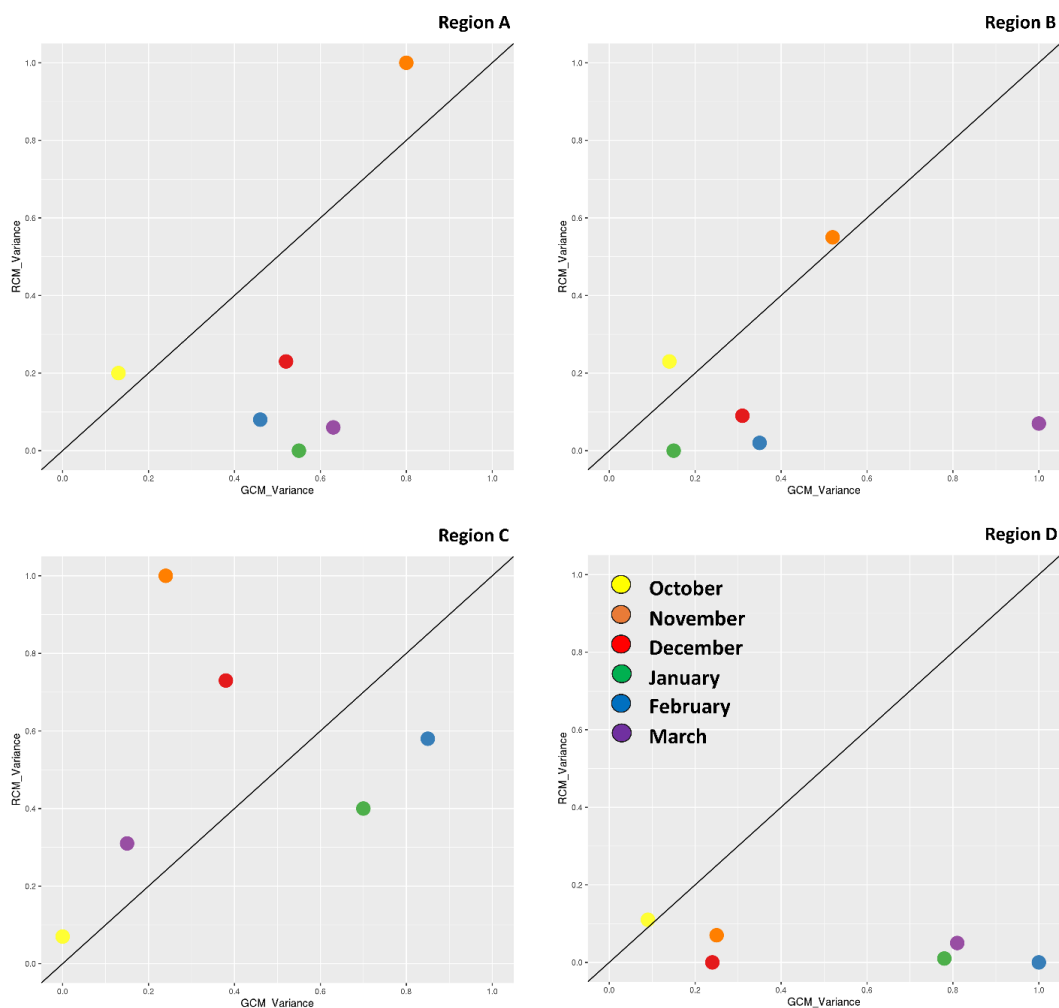
705 **Figure 6.** Scatterplots of the RCM increment (RCM-GCM) for precipitation (mm/day) as a function of the GCM bias  
706 (GCM-OBS) for October. Colors indicate the driving GCM and shapes indicate the downscaling RCMs. The four  
707 panels indicate spatial averages over southern Africa (Region A), the Angola Low region (Region B), the Mozambique  
708 region (Region C) and South Africa region (Region D).



709

710 **Figure 7.** Scatterplots of the RCM increment (RCM-GCM) for precipitation (mm/day) as a function of the GCM bias  
 711 (GCM-OBS) for January. Colors indicate the driving GCM and shapes indicate the downscaling RCMs. The four  
 712 panels indicate spatial averages over southern Africa (Region A), the Angola Low region (Region B), the Mozambique  
 713 region (Region C) and South Africa region (Region D).

714



715

716 **Figure 8.** Analysis of variance for monthly precipitation during 1985-2005 for southern Africa (Region A) and the 3  
717 sub-regions examined, namely Region B (Angola region), Region C (Mozambique region) and Region D (South  
718 Africa region). The x and y-axis display standardized precipitation variances.

719

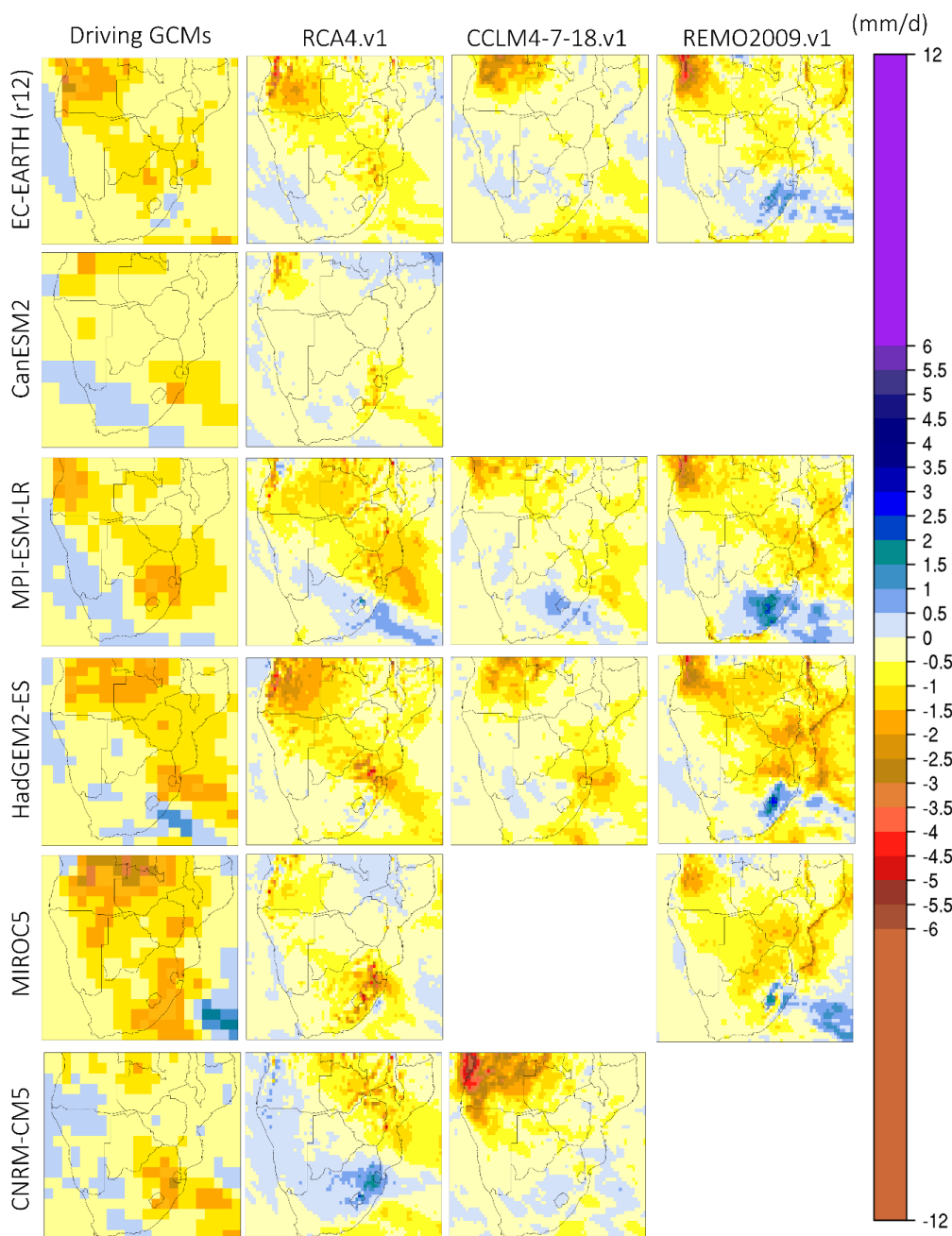
720

721

722

723

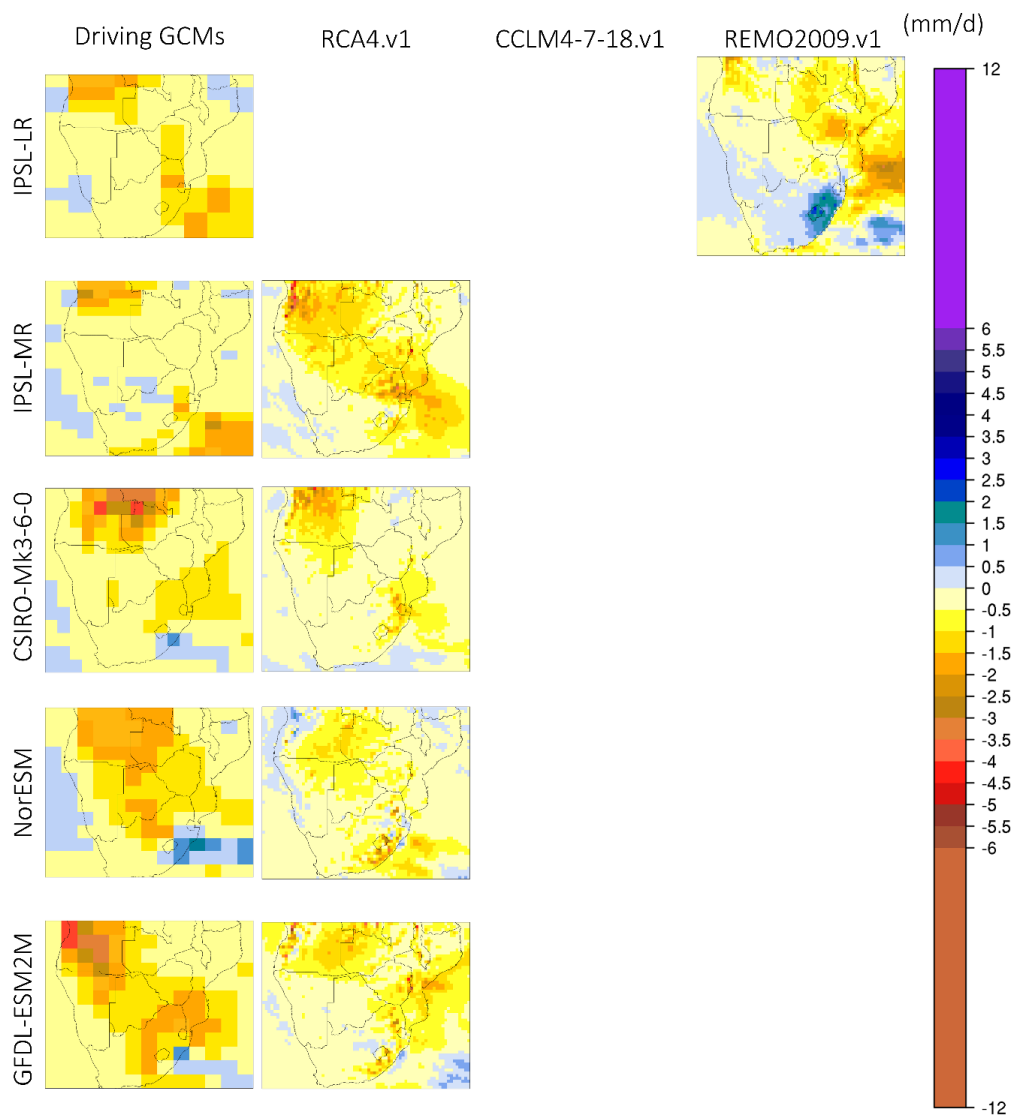
724



725

726 **Figure 9.** Monthly precipitation change (future – present in mm/d) during October for the period 2065-2095 relative to 1985-2005. First column (from the left) displays precipitation change from the driving GCMs used and columns 2-  
727 4 display the downscaled products according to RCA4.v1, CCLM4-8-17.v1 and REMO2009.v1.  
728

729



730

731 **Figure 9.** Continued.

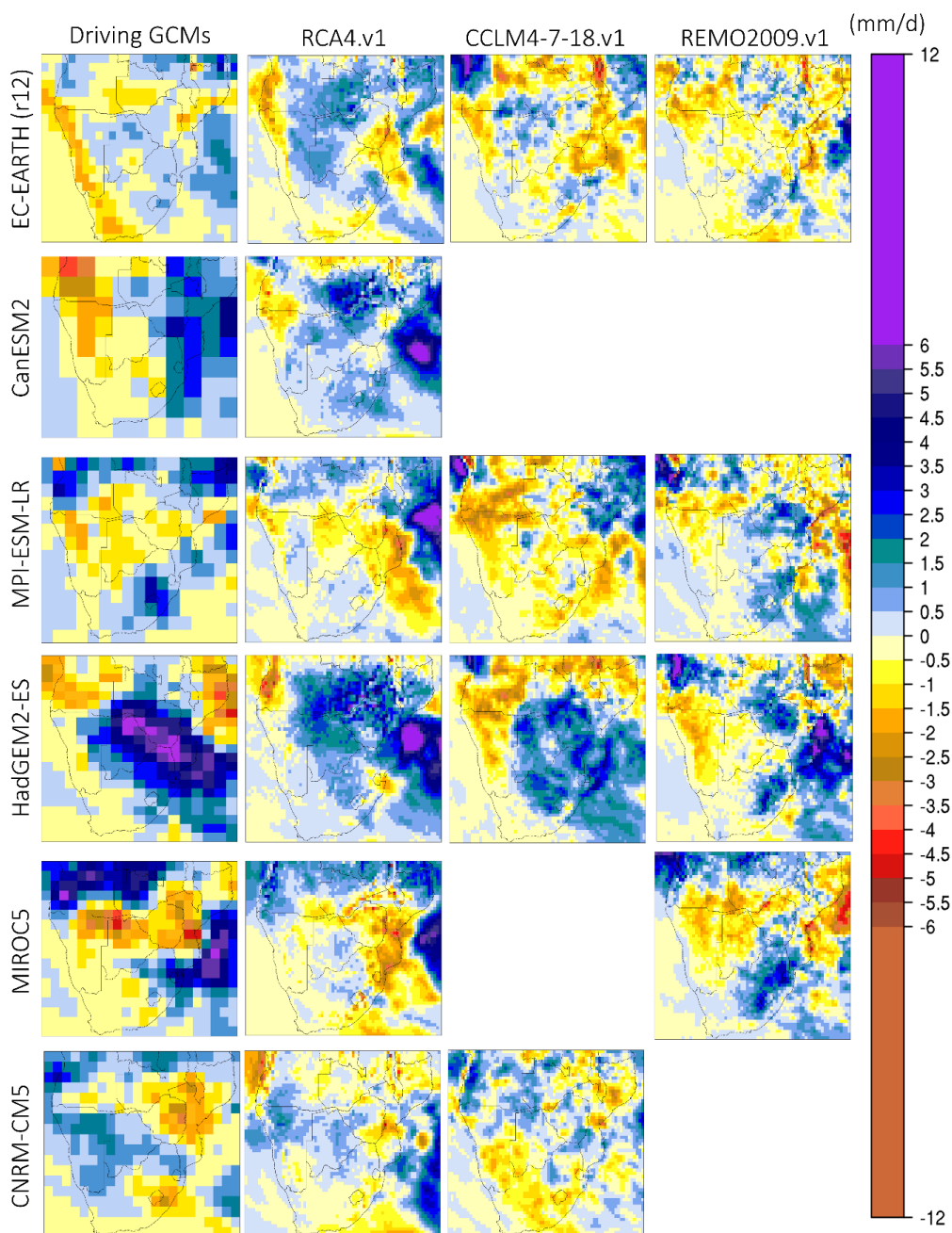
732

733

734

735

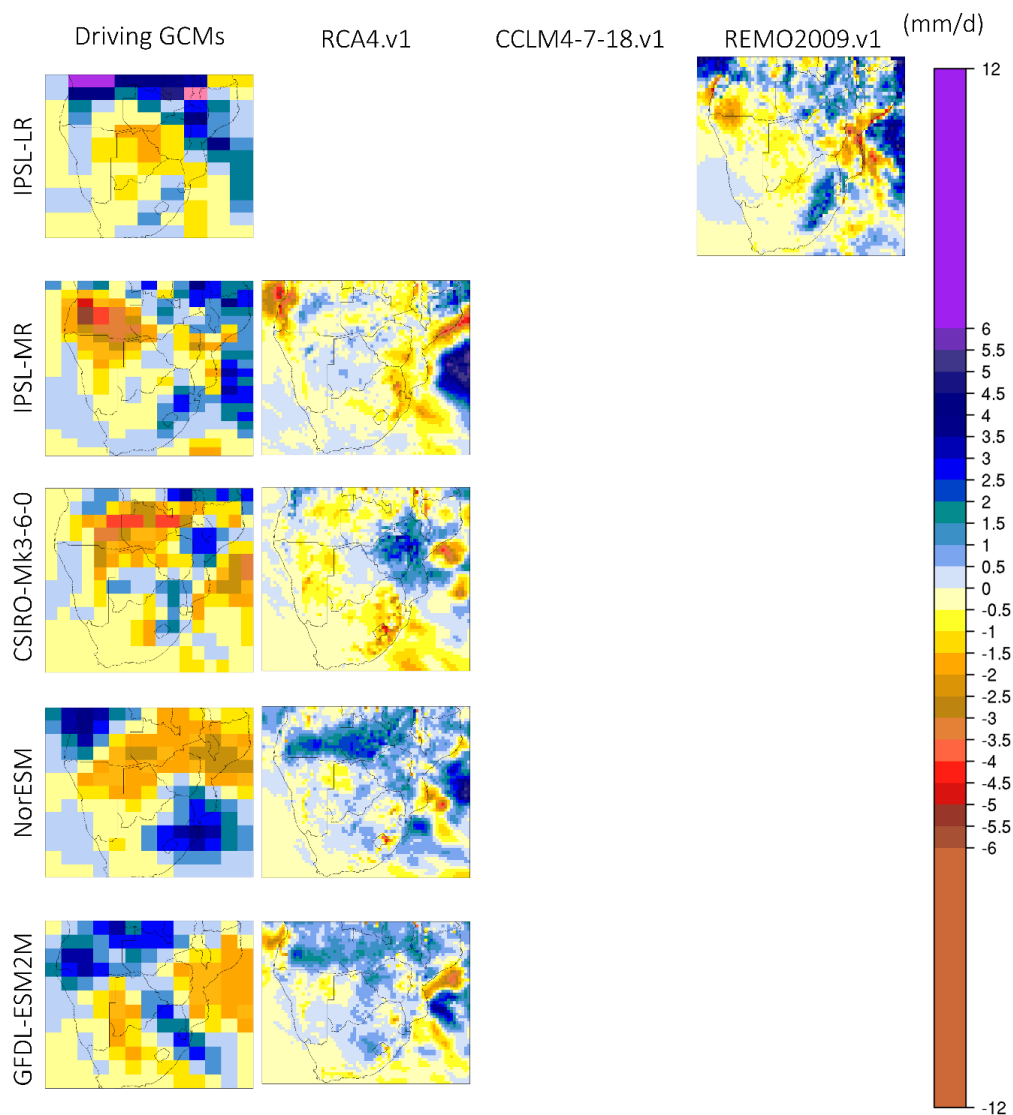
736



737

738 **Figure 10.** Monthly precipitation change (future – present in mm/d) during January for the period 2065-2095 relative  
739 to 1985-2005. First column (from the left) displays precipitation change from the driving GCMs used and columns 2-  
740 4 display the downscaled products according to RCA4.v1, CCLM4-8-17.v1 and REMO2009.v1.

741



742

743 **Figure 10.** Continued.

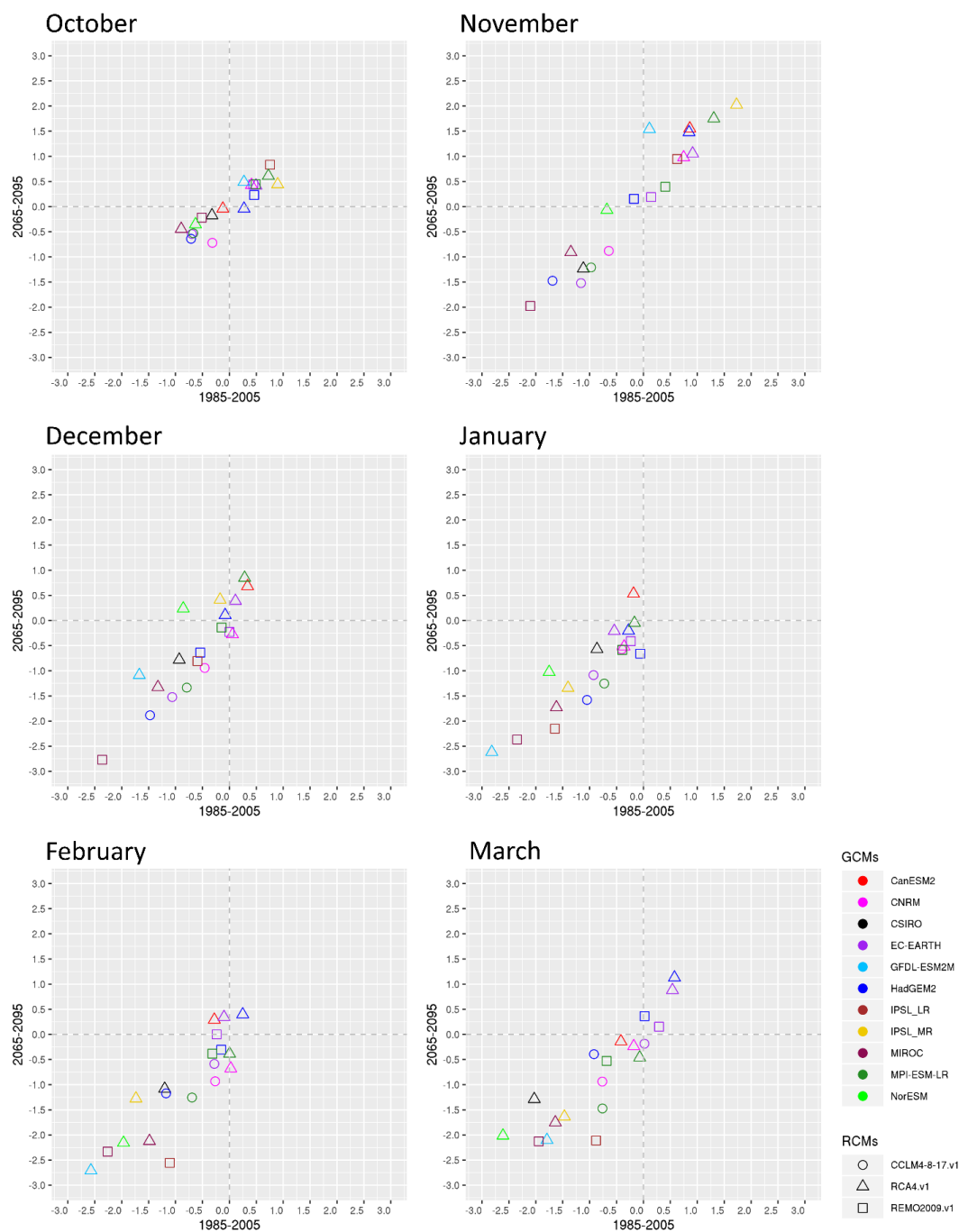
744

745

746

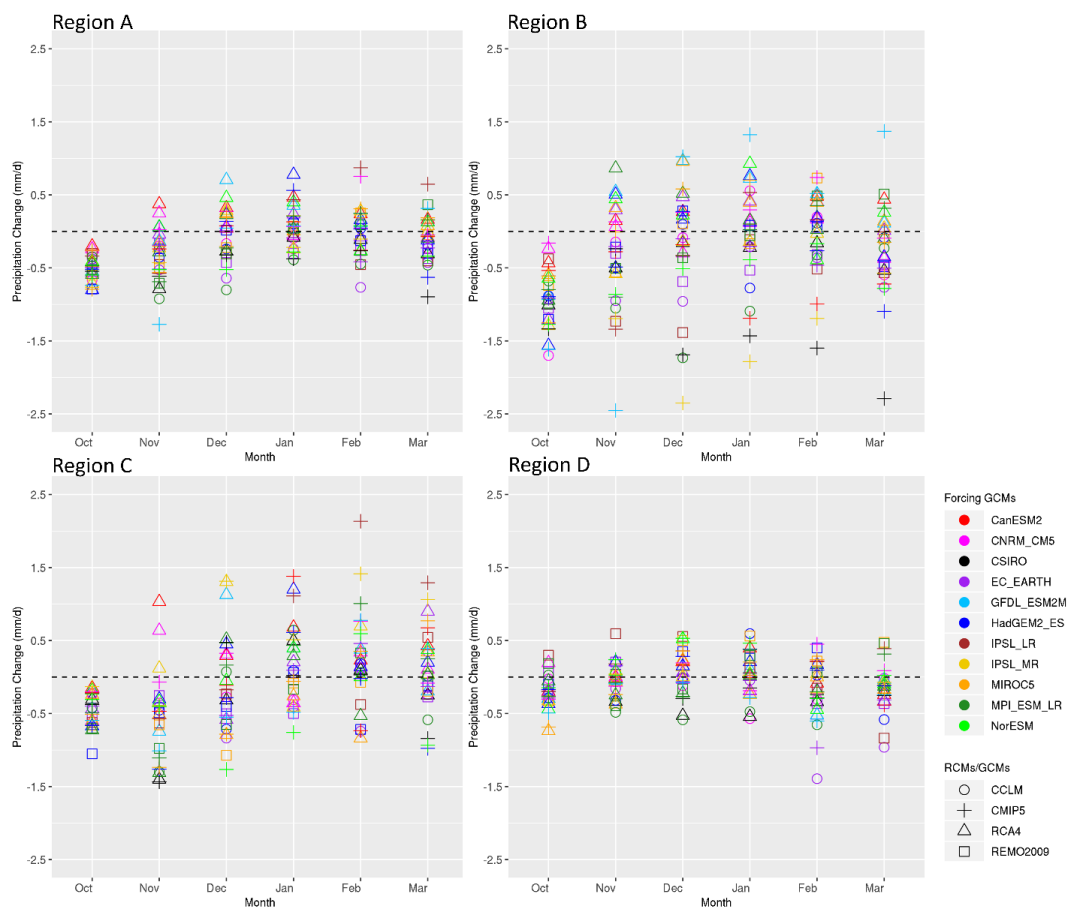
747

748



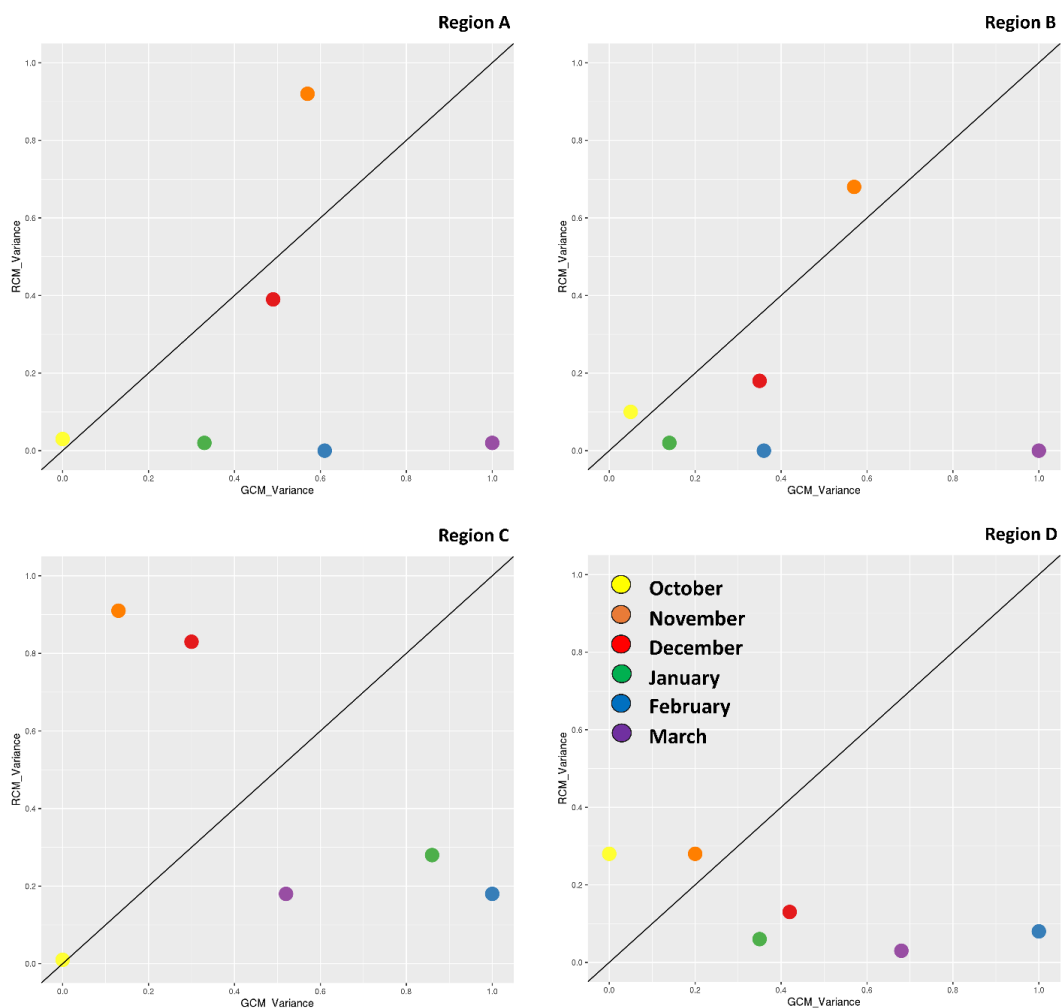
749

750 **Figure 11.** Monthly RCM<sub>DRI</sub> - DRI spatial averages over southern Africa for the historical period (1985-2005) on the  
 751 x-axis and the future period (2065-2095) under RCP8.5 on the y-axis.



752

753 **Figure 12.** Spatial average of the precipitation change signal (mm/d) from RCMs and their driving GCMs relative to  
 754 1985-2005 for southern Africa and the 3 sub-regions examined.



755

756 **Figure 13.** Analysis of variance for monthly precipitation during 2065-2095 for southern Africa (Region A) and the  
757 3 sub-regions examined, namely Region B (Angola region), Region C (Mozambique region) and Region D (South  
758 Africa region). The x and y-axis display standardized precipitation variances.

759

760